PLOS COMPUTATIONAL BIOLOGY

RESEARCH ARTICLE

Building a mechanistic mathematical model of hepatitis C virus entry

Mphatso Kalemera[1], Dilyana Mincheva[2], Joe Grove[1]*, Christopher J. R. Illingworth[2]*

1 Institute of Immunity and Transplantation, Division of Infection and Immunity, University College London, United Kingdom, **2** Department of Genetics, University of Cambridge, Cambridge, United Kingdom

* j.grove@ucl.ac.uk (JG); chris.illingworth@gen.cam.ac.uk (CJRI)

Citation: Kalemera M, Mincheva D, Grove J, Illingworth CJR (2019) Building a mechanistic mathematical model of hepatitis C virus entry. PLoS Comput Biol 15(3): e1006905. https://doi.org/10.1371/journal.pcbi.1006905

Editor: Claus O. Wilke, University of Texas at Austin, UNITED STATES

Received: June 1, 2018

Accepted: February 28, 2019

Published: March 18, 2019

Data Availability Statement: Code is available from https://github.com/cjri/HCVModel. All other relevant data are within the paper and its Supporting Information files.

Funding: This work was funded by The Wellcome Trust (wellcome.ac.uk) and The Royal Society (royal society.org); grant numbers 101239/Z/13/Z (CJRI) and 107653/Z/15/Z (JG). CJRI acknowledges funding from the Isaac Newton Trust. The funders had no role in study design, data collection and analysis, decision to publish, or preparation of the manuscript.

Abstract

The mechanism by which hepatitis C virus (HCV) gains entry into cells is a complex one, involving a broad range of host proteins. Entry is a critical phase of the viral lifecycle, and a potential target for therapeutic or vaccine-mediated intervention. However, the mechanics of HCV entry remain poorly understood. Here we describe a novel computational model of viral entry, encompassing the relationship between HCV and the key host receptors CD81 and SR-B1. We conduct experiments to thoroughly quantify the influence of an increase or decrease in receptor availability upon the extent of viral entry. We use these data to build and parameterise a mathematical model, which we then validate by further experiments. Our results are consistent with sequential HCV-receptor interactions, whereby initial interaction between the HCV E2 glycoprotein and SR-B1 facilitates the accumulation CD81 receptors, leading to viral entry. However, we also demonstrate that a small minority of viruses can achieve entry in the absence of SR-B1. Our model estimates the impact of the different obstacles that viruses must surmount to achieve entry; among virus particles attaching to the cell surface, around one third of viruses accumulate sufficient CD81 receptors, of which 4–8% then complete the subsequent steps to achieve productive infection. Furthermore, we make estimates of receptor stoichiometry; in excess of 10 receptors are likely to be required to achieve viral entry. Our model provides a tool to investigate the entry characteristics of HCV variants and outlines a framework for future quantitative studies of the multi-receptor dynamics of HCV entry.

Author summary

Hepatitis C virus affects approximately 70 million people worldwide, resulting in a significant impact on human health. The virus initiates infection through a complex set of interactions with proteins on the surface of human cells. Here we combine experimental approaches with a new mathematical model to study the process of viral entry. Our model is successful in capturing the behaviour of experiments, which show how changes in the amount of the human proteins CD81 and SR-B1 expressed by a cell alter the probability of a virus getting into a cell. Our model suggests that more than 10 CD81 receptors are

Competing interests: The authors have declared that no competing interests exist.

needed to gain entry into a cell, and shows that viral entry is a difficult task, with many viruses failing at different stages of the entry process. Our model sets out a basis for further quantitative research into the process of HCV viral entry.

Introduction

HCV can establish a lifelong infection and is a leading cause of liver failure, resulting in 350,000–700,000 deaths annually [1]. A molecular understanding of the intermediate stages of viral replication (e.g. RNA replication, protein processing) has allowed the development of potent antivirals capable of curing >95% of HCV infections [2]. However, of the ~70 million HCV positive individuals, the majority do not know they are infected; consequently transmission rates remain high and may even be increasing [3]. A prophylactic vaccine is the greatest unmet need in our response to HCV; progress towards an antibody-based vaccine would be expedited by a molecular understanding of virus entry.

HCV has an enveloped particle that enters via clathrin-mediated endocytosis and low-pH triggered fusion, this process is driven by the glycoproteins E1 and E2 [4]. The molecular events leading up to fusion are only partially understood but are thought to involve at least five essential host factors: CD81, scavenger receptor B1 (SR-B1), epidermal growth factor receptor (EGFR), claudin-1 and occludin [5–9]. However, clear evidence of direct virus-receptor interaction has, at present, only been found for two of these factors: CD81 and SR-B1. The N-terminal hyper-variable region-1 (HVR-1) of the major glycoprotein, E2, forms a linear binding site that interacts with SR-B1 [6,10]. By contrast the CD81 binding site is composed of discontinuous protein domains that are bought together in the tertiary structure of E2 and interact with the large extracellular loop of CD81 [5,11]. Strain specific and broadly neutralising antibodies, which develop during natural infection, act by blocking E2-SR-B1/CD81 interactions [12–15]. A deeper understanding of E2 function and its interactions with SR-B1 and CD81 is likely to aid the design of candidate B-cell targeted vaccines. Moreover, an appreciation of pinch points in the HCV entry pathway may guide the use of entry inhibitor drugs in combination with direct-acting antivirals [16,17].

In common with other viruses [18], HCV entry proceeds in a stepwise fashion, combining three phases. During attachment, viral particles encounter cells via passive diffusion, and attach via multiple low-affinity, low-specificity interactions. During engagement, attached viral particles undergo two-dimensional diffusion across the cell surface, resulting in chance encounters with and binding to bone-fide viral receptors. Finally, viral penetration occurs, leading to the delivery of viral genetic material across the cellular membrane. The whole process is time-limited by the intrinsic instability of the viral particle; entry must be achieved before the virus has passed its 'expiration date' [19,20].

The defined stepwise nature of virus entry makes this process highly amenable to mathematical modelling. Indeed, mathematical modelling has a long history of generating insight into processes of viral infection [21]. For example, a model of receptor expression and viral entry was combined with experimental data to show that binding to more than one Tva800 molecule is required for avian sarcoma leukosis virus to achieve entry [22].

Concerning HCV, modelling approaches have been used to investigate the basic evolutionary properties of the virus [23], its spread between cells [24], and the effectiveness of a variety of viral therapies [25–27]. Previous modelling studies of HCV entry have utilised a model whereby contact between a virus particle and the cell membrane leads to the formation of a stochastic number of E2-CD81 complexes, with viral entry occurring on the formation of a

given number of complexes. This model has been used to estimate that between 1 and 13 complexes are required for entry [28], and further developed to explain changes in the cellular expression of claudin-1 following HCV infection [29].

Here we combine experimental data with a novel mathematical model to evaluate the relationship between the HCV protein E2 and the cellular receptors SR-B1 and CD81. Using basic virological assays we measured attachment and receptor engagement by HCV. These observations, combined with previous literature, allowed us to construct a putative minimal model for HCV entry, which we parameterised using the collected experimental data. Our model supports the notion of sequential receptor interactions by HCV, with initial engagement of SR-B1 likely performing a priming function to enhance CD81 interactions. Our model is robust, achieving an excellent fit with the experimental data describing viral entry. The model offers estimates of receptor stoichiometry and the efficiency of HCV entry, and provides a tool for future investigations of E2 glycoprotein function.

Results

To assess HCV viral entry we use a combined experimental and mathematical approach, first of all conducting experiments to assess the role of CD81 and SR-B1 in viral entry before using this data to build and refine a mathematical model. To achieve this we exploited the HCVcc system; HCV particles generated *in vitro* were used to infect human hepatoma cell lines. This system is tractable and manipulable, and generates highly reproducible data [30,31].

Measurement of viral attachment

A virus attachment assay showed that only a minority of virus particles used in our experimental setup attached to Huh-7.5 cells. Viral inoculum was added to wells of an assay plate containing human hepatoma cells (Huh-7.5 or Huh-7). After five hours the number of virus particles associated with the cells was evaluated by qPCR quantification of genome copy numbers (Fig 1). Wells containing human hepatoma cells adsorbed significantly more virus than empty control wells (~17,000 RNA copies, compared to ~6000); we interpret the difference between these values as representing true levels of virus attachment (i.e. ~11,000 particles). To investigate the potential role of entry receptors in attachment, we also quantified the association of particles with Huh-7 cells in which SR-B1 or CD81 had been genetically ablated by CRISPR Cas9 gene editing. We observed no defect in virus attachment to these cells when compared to parental Huh-7 cells; this is in agreement with a previous study and is consistent with the notion of virus attachment being largely independent of receptor engagement [32–34]. From our measurements we deduced that only ~5% of the experimental inoculum attached to the cells. This apparent bottleneck is likely due to the limited speed of virus particles diffusing in the inoculum volume (100μl); in our setup the majority of virus particles in a well are unlikely to even encounter a cell [35].

Receptor availability and viral entry

Antibody-mediated blockade experiments showed a decrease in viral entry with decreasing availability of the CD81 and SR-B1 receptors. The basic workflow of our infection assay is summarised in S1 Fig. Huh-7.5 cells were pre-incubated with anti-SR-B1 or anti-CD81 antibodies that are capable of inhibiting E2-receptor interaction and preventing infection [35–37]. The blockaded cells were then challenged with HCV and infectivity was assessed after 48 hours. In a parallel assay plate, antibody binding was assessed by fluorescence microscopy, allowing us to evaluate receptor availability during the virus challenge. A serial dilution of each antibody revealed saturation of binding at high concentrations, suggesting complete receptor

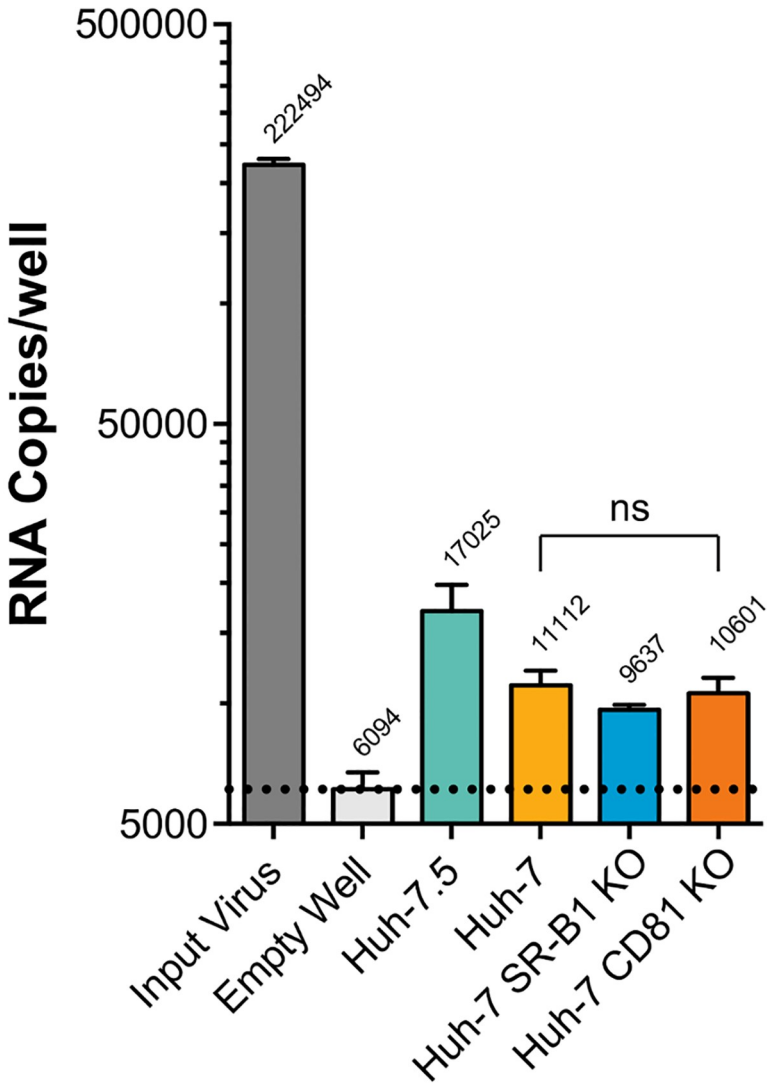

Fig 1. A minority of input virus particles attach to target cells. HCV was inoculated in to replicate wells of a 96 well plate containing the specified cell lines. After five hours the wells were washed with PBS and bound HCV was quantified by qPCR. Each well received >200,000 RNA copies, in an empty well <3% of these remain after washing. Wells containing cells bound significantly more virus than empty wells (p = 0.02–0.008). Huh-7 cells that had been gene-edited to remove SR-B1 or CD81 displayed no significant difference in virus attachment, when compared to parental Huh-7 cells. The data suggests that ~5% (~11,000 copies) of the input HCV inoculum binds to Huh-7.5 cells. The dashed line indicates the background level of virus binding in empty control wells. Mean values of n = 3 independent experiments are shown. Error bars indicate the standard error of the mean. Statistical analysis performed using an unpaired t-test (GraphPad Prism).

https://doi.org/10.1371/journal.pcbi.1006905.g001

blockade; i.e no receptors were available for entry (Fig 2A and 2B). Our results show a clear difference between the two receptors; while an absolute blockade of CD81 completely prevented infection, a similar blockade of SR-B1 allowed a small proportion of viruses to achieve infection (Fig 2C). These results suggest that CD81 is absolutely necessary for HCV entry, (consistent with many reports [8,30,38,39]), while SR-B1 is not strictly necessary for entry to occur. Further support for this conclusion was obtained from measurements of HCV infection of receptor knock-out cells (S2 Fig); modest infection occurred in SR-B1 KO cells, whereas no

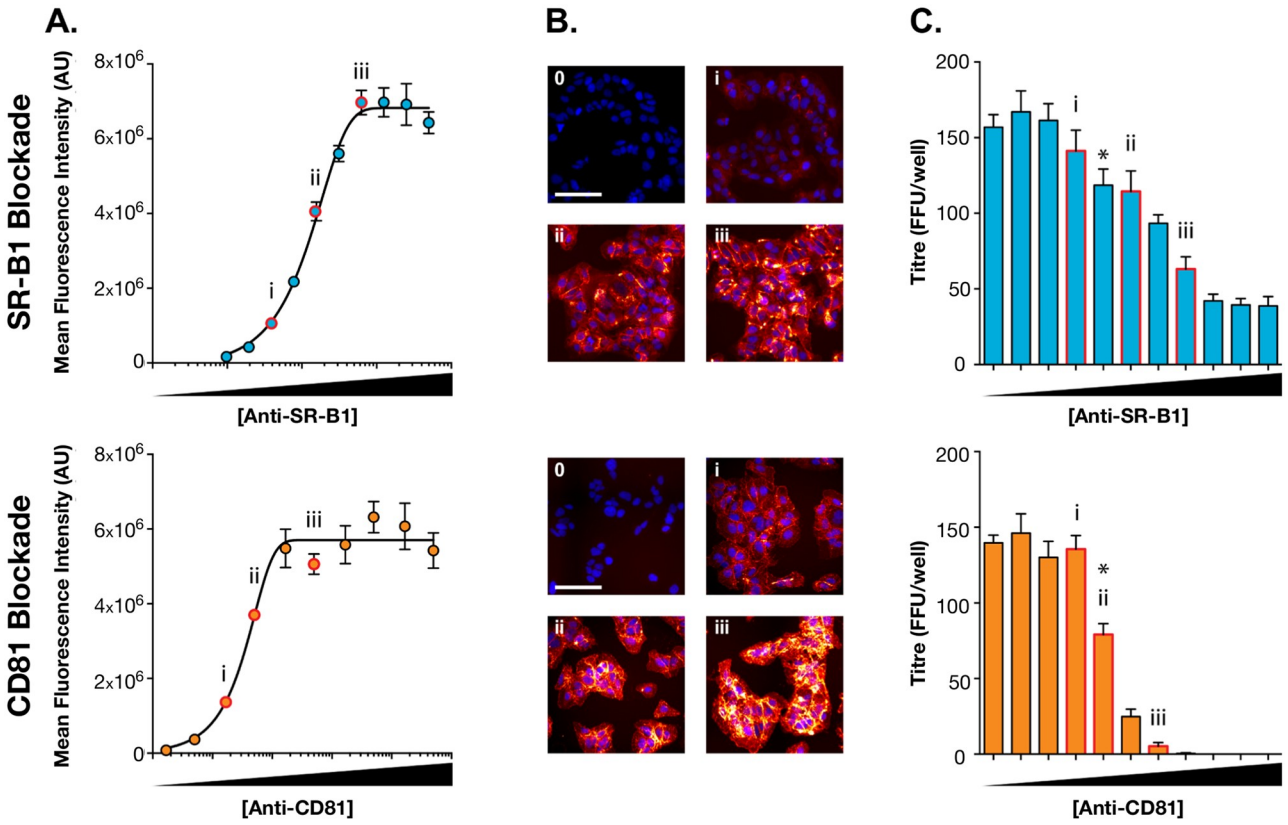

Fig 2. Receptor blockade reveals an SR-B1 independent mode of infection. Huh-7.5 cells were pre-incubated with a dilution series of rabbit anti-SR-B1 serum or anti-CD81 monoclonal supernatant and then challenged with HCVcc. **A**. Binding of anti-receptor antibodies was quantified using fluorescence microscopy, receptor saturation was achieved at high antibody concentrations. Data points represent mean values of n = 3 replicates, error bars indicate standard error of the mean. Data was fitted using a sigmoidal curve in GraphPad Prism. **B**. Example fluorescent micrographs of labelled cells, the images are representative of the annotated data points in A. Scale bar 50μm. **C**. HCV infectious titre, expressed as foci per well, in receptor blockaded Huh-7.5 cells, annotated as in A. and B. Complete blockade of CD81 prevents HCV infection, whereas a minority of infection prevails in SR-B1 blockaded cells. Bars represent mean values of n = 4 technical replicates, error bars indicate the standard error of the mean. Asterisk indicates the point at which titre becomes significantly different from untreated cells (unpaired t-test, GraphPad Prism). Data from one representative experiment is shown, subsequent modelling was performed with n = 3 independent experiments.

https://doi.org/10.1371/journal.pcbi.1006905.g002

infection was detected in the absence of CD81. This indicates that a small proportion of virus particles achieve entry in an SR-B1 independent manner [8,30,39].

Over-expression of SR-B1 and CD81 in cells showed an increase in viral entry with increasing receptor availability. Lentiviral vectors were used to introduce additional receptor coding genes to Huh-7.5 cells. These cells were then challenged with virus as described above (S1 Fig). Parallel plates were fixed and stained for fluorescence microscopy, allowing us to evaluate receptor availability during the virus challenge. Lentiviral transduction resulted in up to four times greater expression than parental cells (Fig 3A). In addition to the receptor coding sequence, the lentiviral vectors also encode GFP, expressed from an additional promoter. Therefore, as an independent measure of transduction, we evaluated GFP expression (S3 Fig); this revealed that all cells were expressing comparable levels of GFP, suggesting homogenous transduction. This is important for unambiguous interpretation of the infectivity data. Whilst infection levels were not directly proportionate to receptor expression, lentiviral transduction resulted in a significant, and dose responsive, increase in HCV infection (Fig 3C). Taken together, the blockade and over-expression data indicate that SR-B1/CD81 availability limits HCV infection.

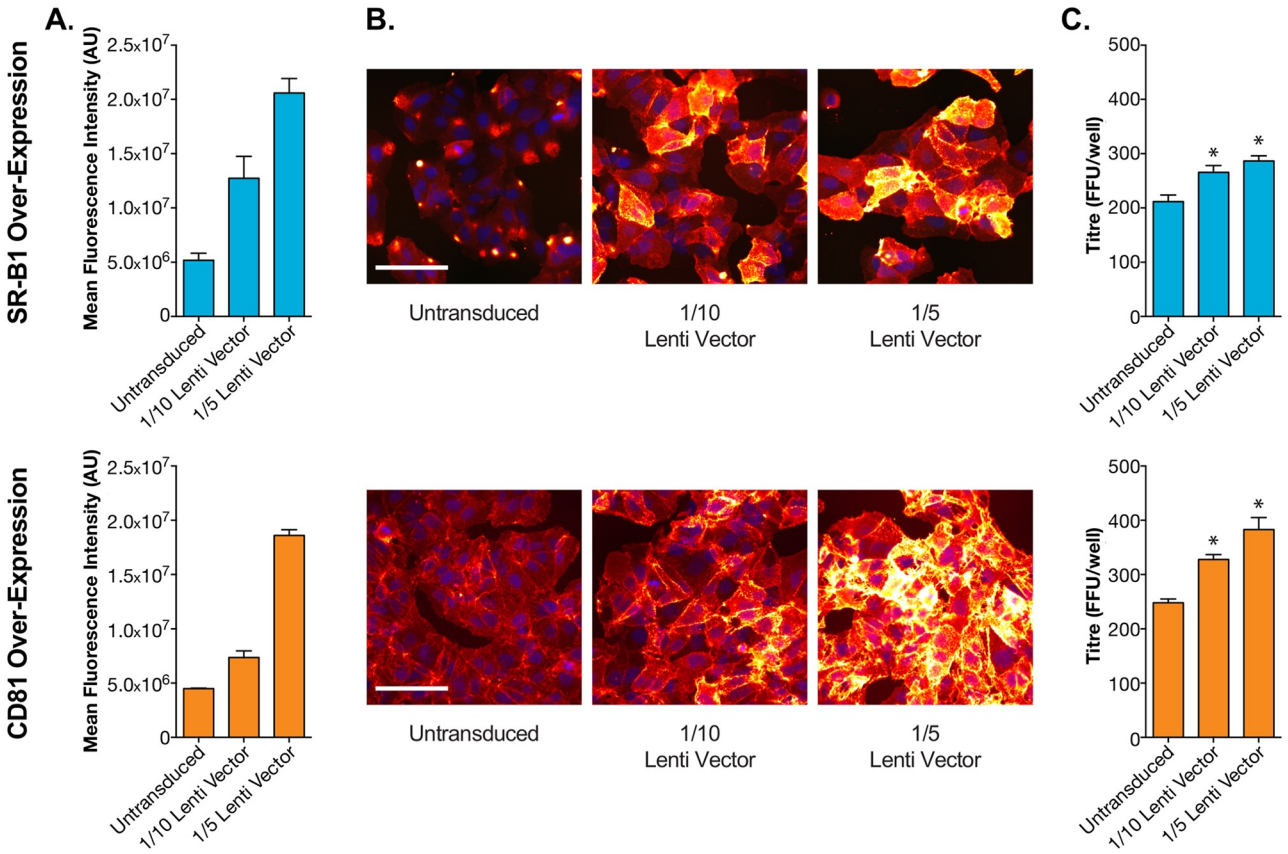

Fig 3. Receptor over-expression enhances HCV infection. Huh-7.5 cells were transduced with lentiviral vectors expressing exogenous human SR-B1 or CD81 and then challenged with HCVcc. **A**. Receptor over-expression was quantified using fluorescence microscopy. Bars represent mean values of n = 4 technical replicates, error bars indicate standard error of the mean. **B**. Example fluorescent micrographs of cells over-expressing receptor. Scale bar 50μm. **C**. HCV infectious titre, expressed as foci per well, in receptor over-expressing Huh-7.5 cells. Bars represent mean values of n = 4 technical replicates, error bars indicate standard error of the mean. Data from one representative experiment is shown, subsequent modelling was performed with n = 3 independent experiments. Asterisks indicate significant difference from untreated cells (unpaired t-test, GraphPad Prism).

https://doi.org/10.1371/journal.pcbi.1006905.g003

Assessment of virus-receptor interactions

Soluble E2 binding assays suggested that the interaction affinity between E2 and SR-B1 is greater than that between E2 and CD81. Experiments were conducted to measure the binding of recombinant soluble E2 glycoprotein (sE2) to cell surface expressed receptor. This provides a direct measure of virus-receptor interaction, albeit in an artificial system where the components are not presented in their native context.

Chinese hamster ovary (CHO) cells do not bind HCV E2 glycoprotein, however, sE2 binding can be conferred by introduction of exogenous human SR-B1 or CD81; this was measured by flow cytometry. We treated CHO cells with the receptor + GFP lentiviral vectors (as described above). Antibody staining revealed high levels of receptor expression in GFP positive cells (S4 Fig), with no receptor expression in the minority population of untransduced GFP negative cells. Saturation of binding was achieved at high concentrations of anti-receptor antibody; the intensity of fluorescent signal suggested comparable expression levels for SR-B1 and CD81 (Fig 4A and 4B). In parallel samples, cells were also incubated with a serial dilution of sE2; example raw fluorescent intensity data is provided in (S5 Fig). sE2 binding to CHO-SR-B1 cells was robust (Fig 4C and 4D), whereas binding to CHO-CD81 cells was poor. Given the

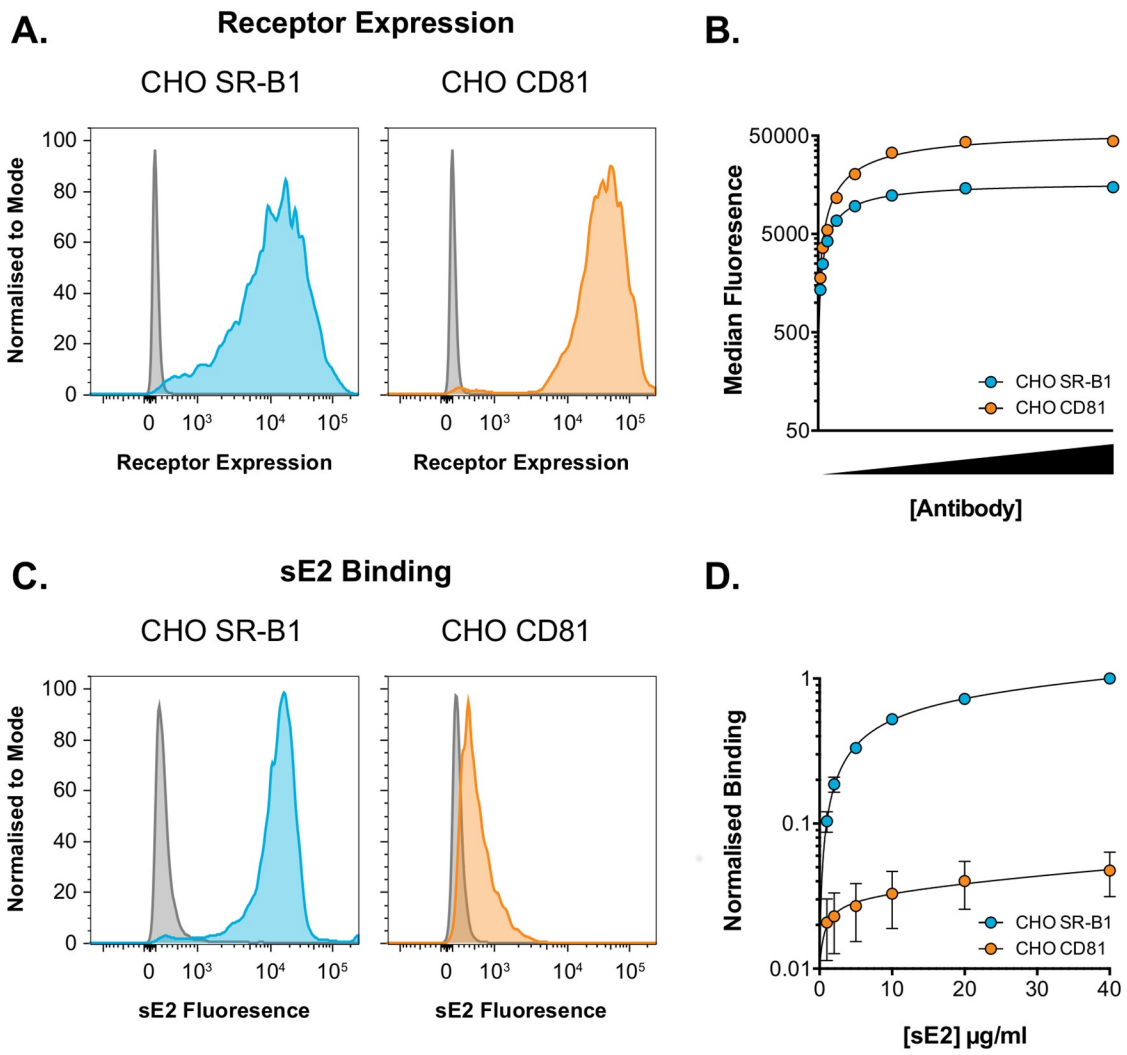

Fig 4. Soluble E2 binds more readily to SR-B1 than CD81. CHO cells were transduced with lentiviral vectors expressing human SR-B1 or CD81 and then used in a sE2-binding assay. **A**. Representative flow cytometry histograms of cell surface expression of HCV receptor in CHO cells, grey plots are untransduced control cells. **B**. Transduced CHO cells were incubated with a serial dilution of anti-receptor antibody. Antibody binding was quantified by flow cytometry; high concentrations of antibody were able to saturate receptor. Data from one representative experiment is shown, data points represent mean values of n = 2 technical replicates, error bars indicate standard error of the mean. **C**. Representative flow cytometry histograms of sE2 binding to CHO cells expressing HCV receptor, grey plots are untransduced control cells. **D**. Transduced CHO cells were incubated with a serial dilution of sE2. sE2 binding was quantified by flow cytometry, high concentrations of sE2 approached saturation of binding. Data is normalised to 40µg/ml sE2 binding to CHO SR-B1 cells. Data points represent mean values of n = 3 independent experiments, error bars indicate standard error of the mean. Data was fitted using a one-site binding curve in GraphPad Prism.

https://doi.org/10.1371/journal.pcbi.1006905.g004

weak binding of sE2 to CHO-CD81 cells, further demonstration of the specificity of sE2 binding to these cells is shown in S6 Fig.

CD81 and SR-B1 receptors had similar expression in CHO cells (Fig 4B). As such, the binding curves obtained from this experiment (S5 Fig and Fig 4D) suggest that the intrinsic level of sE2 binding to SR-B1 is between 20 and 60 times greater than that to CD81. However, these observations must be interpreted with care: this assay uses a soluble truncated form of E2, which is devoid of its partner glycoprotein E1 and is no longer presented on the surface of a virus particle. While data from these experiments was used during model fitting, the

relationship between these results and the viral entry data, is not straightforward; we consider this issue further in the Discussion.

Mathematical model formulation

A mathematical model was used to explain the effect of CD81 and SR-B1 availability upon viral entry. Drawing on the experimental data presented here and past literature [7,40–43] we constructed a minimally complex mechanistic model of HCV receptor engagement (Fig 5A). In our model, once attached to the cell surface, a virus particle must acquire a certain number of CD81 receptors to achieve entry. Prior to binding this number of receptors entry cannot occur, while once sufficient receptors are bound the downstream process of viral entry begins. The number of CD81 receptors required for entry is unknown, but is characterised by a parameter, r, in our model. Models with different numbers of required receptors were compared, allowing us to explore the CD81 stoichiometry of HCV entry.

Our model describes the receptor engagement phase of entry, which occurs after particle attachment (Fig 5A). Acquisition of CD81 by the E2 glycoprotein proceeds via two routes (Fig 5C). The principal route to CD81 acquisition is via SR-B1. In this case, E2 gains SR-B1 through its intrinsically strong binding capacity (Fig 4); this interaction confers an enhanced ability to acquire CD81, possibly through specific priming of E2-CD81 interactions. The second route utilises the low intrinsic binding capacity of E2 for CD81 (Fig 4); in the absence of SR-B1 this pathway will allow a minority of particles to achieve entry (as demonstrated in Fig 2 and S2 Fig). Thus, whilst SR-B1 is unnecessary for viral entry, it significantly increases the rate at which viruses enter the cell. Having acquired sufficient numbers of CD81, HCV particles progress to further stages of virus entry, including the acquisition of downstream receptors, endocytosis and fusion [4,38].

This putative entry mechanism was formulated in terms of a minimally complex mathematical model, which is summarised in Fig 5B. Viruses attached to the membrane are modelled as being in one of a number of states, $M(a,b)$, representing a virus particle that has acquired a CD81 molecules and b SRB1 molecules; upon initial attachment to the membrane the virus occupies the state $M(0,0)$. Each virus has some finite number of E2 proteins, given by N_e, which may bind to SR-B1 and CD81 receptors. E2 proteins bind SR-B1 receptors at some inherent rate s, with the total rate of acquisition of receptors scaling by the number of E2 proteins remaining. We suppose that binding SR-B1 'primes' E2, changing its interaction with CD81. As such, E2 proteins bind CD81 receptors at the intrinsic rate c_1 if they have not been primed by SR-B1, and at the rate c_2 if they have been primed by SR-B1; again the total rate of gain of CD81 is scaled by the number of remaining E2. Having gained sufficient CD81, a virus proceeds through the further steps required to produce an infection at some rate e. During all stages before causing a productive infection viruses die at some 'death' rate d; this models the inherent instability of HCV particles [19,20].

To integrate experimental data on receptor availability (Figs 2 and 3), the model allows CD81 and SR-B1 availability to be scaled by the terms p_c and p_s, respectively, which are expressed relative to unmodified cells. For example, a value of 0.1 would be equivalent to a 90% reduction in receptor availability (via antibody blockade, Fig 2), whereas a value of 2 is achieved by doubling the amount of receptor (via over-expression, Fig 3). To evaluate our model, we used experimentally-determined values for receptor availability and productive infection (Figs 2 and 3). Without loss of generality, the value of d was set to an arbitrary value, all other parameters being calculated relative to this. We then optimised the parameters N_e, s, e, c_1, and c_2 so as to achieve a best-fit model to the data obtained from our experiments. Data describing the effects of SR-B1 and CD81 receptor availability were fitted simultaneously.

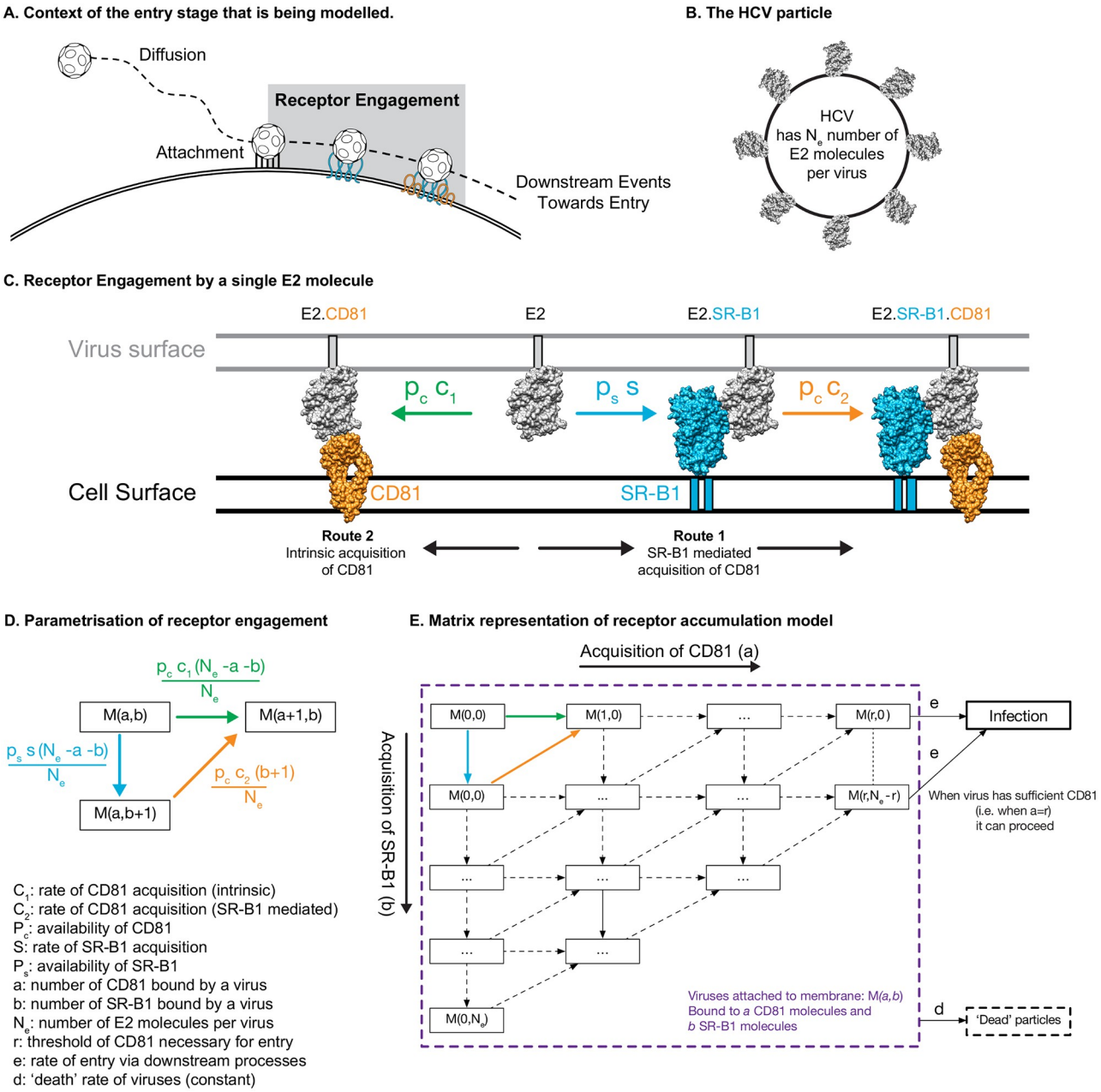

Fig 5. Building a mechanistic model of HCV entry. A. Following attachment HCV particles must engage and accumulate CD81 to proceed to entry. **B**. To model this process we must consider a HCV particle that has an unknown (N_e) number of E2 molecules. **C**. We modelled E2 receptor engagement to occur via two routes: 1. prior engagement of SR-B1 enhances E2 interaction with CD81 2. acquisition of CD81 via intrinsic binding, with no prior involvement of other receptors. The molecular models are drawn to scale and are based on published crystal structures (E2 PDB:6MEJ; CD81 PDB:5TCX; SR-B1 homology model based on PDB:4F7B [56,63,64]) **D**. A parameterised mathematical framework of receptor engagement. Each box represents the receptor engagement state of cell-attached viruses (*M*), where the values in parentheses denote receptor number. For example, *M (0,0)* represents viruses that have attached but have not yet engaged either receptor, *M(1,0)* represents viruses that have acquired one molecule of CD81 and *M(0,1)* are viruses with one molecule of SR-B1. The steps in this process have been parameterised to include the availability of receptor (determined by experimental data) and the rate of engagement (estimated by modelling). They have also been scaled relative to the number of available E2 molecules (N_e). For clarity, parameterised steps are also shown in C. **E**. A matrix model of HCV receptor accumulation. To achieve productive infection (*I*) virus particles must move laterally, acquiring CD81, this is achieved via the routes defined in D. The dimensions of this matrix represent the stoichiometry of receptor engagement (i.e. how many molecules of CD81 are required for entry), we investigated this through the modelling process. There are two additional parameters in the model, *e* integrates all downstream events in the virus life cycle leading to productive infection, whereas *d* is the rate of spontaneous virus inactivation, or 'death'.

https://doi.org/10.1371/journal.pcbi.1006905.g005

It must be noted that a report by Yamamoto et. al. suggests that there is a level of redundancy in HCV entry whereby LDLR can perform analogous functions to SR-B1 [39]. This raises the possibility that LDLR participates in route 2 of our model, providing a priming step for CD81 interaction (S8A Fig). Experimental evidence suggested that while LDLR plays a role in HCV viral entry, it does not substitute for SR-B1 in our model. Targeting LDLR by antibody blockade or genetic knockout led to the inhibition of HCVcc infection (S8B and S8C Fig), albeit to a lesser extent than SR-B1 targeting. We reasoned that if there is a redundancy in function we would expect a synergy between SR-B1 and LDLR receptor blockade; in other words, if the SR-B1 route is unavailable HCV entry will proceed solely along the LDLR route, making LDLR blockade a more effective treatment. However, when used in combination anti-SR-B1 and anti-LDLR reduced viral entry in an additive fashion (S8D Fig). Moreover, increasing the concentration of anti-SR-B1 had no effect on the net inhibitory action of anti-LDLR (S8E Fig). This lack of synergy is strong evidence that LDLR does not function in an analogous manner to SR-B1 and is likely to be contributing to virus entry either upstream or downstream of receptor engagement.

Model outputs and predictions

Our model estimates the probability that a single virus founds a productive infection under varying availability of CD81 and SR-B1. Conversion of this statistic to the probability that a single cell is infected in the assay of S1 Fig was obtained by accounting for the number of attached virus particles in the experiment (Fig 1).

Optimisation of model parameters gave an excellent fit to the experimental data (Fig 6). Inferences from our model further characterise the fate of virus particles: close to one in three of the HCV particles which attach to the membrane acquire a sufficient number of CD81 molecules to proceed with virus entry. Downstream events leading to productive infection are then even less efficient, with close to 4% of particles which gain sufficient CD81 completing

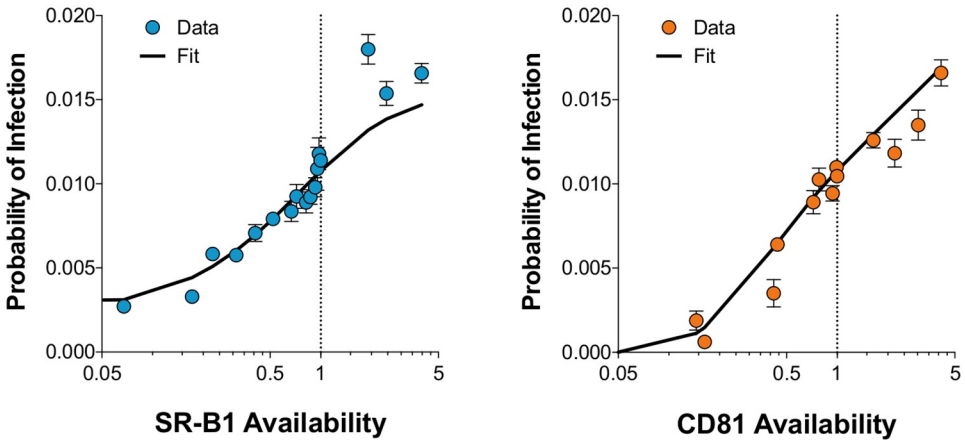

Fig 6. The mathematical model achieves excellent fit with experimental data. Multiple independent receptor blockade/over-expression experiments allowed us to determine the relationship between receptor availability and HCV infectivity. By integrating the virus attachment data from Fig 1 we estimated the probability of an attached virus yielding a productive infection for each condition. The X-axis represents receptor availability where values below 1 are derived from receptor blockade experiments and values above 1 are from over-expression experiments. The Y-axis displays the probability of a cell within the experimental setup being infected by virus. The data points display mean probability of infection under varying receptor availability from n = 3 independent experiments (for both receptor blockade and over-expression, i.e. n = 6 experiments in total). Error bars indicate standard error of the mean. The black line displays the fit achieved with the model optimised; the data and fit are in excellent agreement.

https://doi.org/10.1371/journal.pcbi.1006905.g006

Table 1. Optimised model outputs. This table displays optimised values for the critical model parameters outlined in Fig 5. Outputs are shown for the primary model (presented throughout this report) and three variant models; CD81/SR-B1 unbinding models are based on the primary model but also allow for receptor dissociation, for these models the optimised dissociation rate is given in parentheses; in the null model SR-B1 binding does not affect the rate of CD81 acquisition, in this case parameter s (annotated by asterisk) is optimised purely using the sE2 binding data. The models can also be used to predict the fate of membrane bound virus particles. Here, we provide the inferred proportion of viruses that acquire sufficient CD81, that complete downstream steps of entry and that achieve productive infection.

	Primary Model	CD81 Unbinding	SR-B1 Unbinding	Null Model
Peak Likelihood	-3121	-3122	-3091	-3850
Optimised parameters				
Intrinsic ability to acquire SR-B1 (s)	**0.58**	0.58	0.7 (0.57)	9*
Intrinsic ability to acquire CD81 (c_1)	**0.24**	0.24 (0)	0.15	0.39
Primed acquisition of CD81 (c_2)	**1.36**	1.35 (0)	12.9	n/a
Likely stoichiometry	**>10**	>10	>4	>4
Predicted entry efficiency in unmodified cells				
Proportion of particles that acquire sufficient CD81	**36.8%**	36.7%	32.71%	59.7%
Proportion of particles that complete downstream events	**3.9%**	3.8%	4.35%	2.2%
Proportion of particles that achieve infection	**1.4%**	1.4%	1.42%	1.32%

https://doi.org/10.1371/journal.pcbi.1006905.t001

these steps. Consequently, a virus particle participating in an infection assay has a very small chance of success: only ~5% of particles attach to the membrane (Fig 1) with only ~1.4% of these achieving productive infection (Table 1). Related to this, the fits shown in Fig 6 do not appear to plateau, suggesting that further increases in receptor expression would continue to enhance infection. Given further increases in receptor availability we would expect this to saturate, either because all viral particles acquire sufficient CD81 or as inefficiencies in downstream entry events limit particle infectivity.

Precise inference of receptor stoichiometry was not possible from our model, which showed an increasing likelihood with a greater number of CD81 receptors being required for viral entry. However, multiple receptors appear to be required; likelihood outputs from our model suggested that more than 10 receptors are needed for entry. Comparison of models with differing numbers of available E2 proteins favoured an explanation in which the number of E2 proteins was close to the number of CD81 receptors required for entry.

Inferences from our model showed a smaller difference between the intrinsic binding propensities for CD81 and SR-B1 than indicated from the sE2 binding experiments; while the experiments with soluble E2 suggested a ratio in excess of 20, our model inferred a 2-fold to 3-fold preference for SR-B1. Re-running the inference calculation in a manner that ignored the contribution of the sE2 data gave a very similar set of inferred parameters, suggesting that these data had little influence on our model output (S1 Table).

Investigating receptor interdependency

Our model predicts a specific interdependence in HCV receptor usage that we can confirm experimentally. We used the model to investigate the effect of co-varying SR-B1 and CD81 availability; in effect, this enables *in silico* infection assays to be performed with arbitrary receptor availability (Fig 7A).

An evaluation of the predictive power of our model suggested that the extent of the influence of SR-B1 may have been underestimated by our basic model fit. In an experimental test, CD81 availability was increased by lentiviral transduction to achieve a ~3 fold increase in surface expression. These cells were then subjected to anti-SR-B1 receptor blockade, so as to evaluate SR-B1 dependence. Fig 7B displays the predicted outcome along with empirical measurements from this experiment. To aid comparison the data is presented as % inhibition

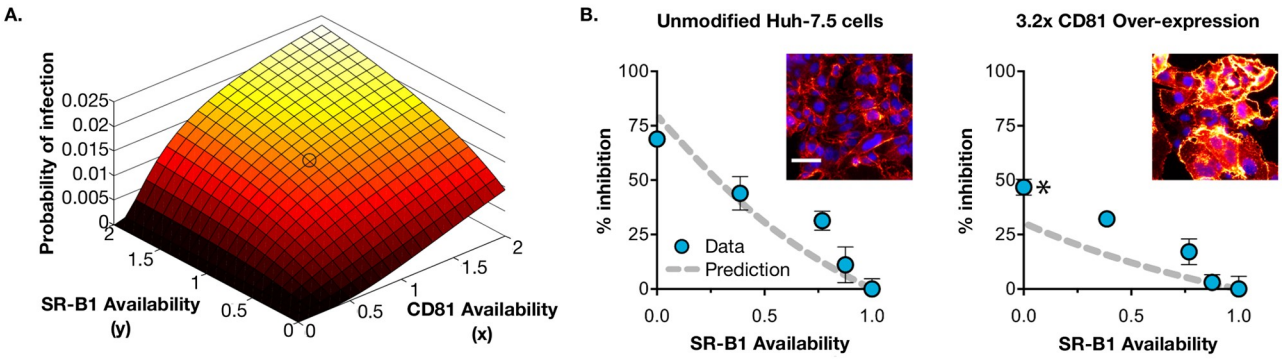

Fig 7. Experimental verification of model predictions. Our mechanistic model can be used to predict the probability of infection for any given availability of SR-B1 or CD81. **A**. Surface plot demonstrating the effect of co-varying receptor availability from 0–2, the circled area indicates the probability of infection in unmodified cells. Note that in the absence of CD81, altering SR-B1 levels has no effect; in contrast increased CD81 availability is able to rescue infectivity in cells lacking CD81. We experimentally tested this relationship between CD81 expression and SR-B1 dependence. **B**. Inset micrographs display CD81 and DAPI stained samples of unmodified Huh-7.5 cells or those transduced with lentivirus encoding CD81; 3.2x over-expression was achieved. Scale bar 50μm. We investigated SR-B1 dependence in the over-expressing cells by antibody-mediated receptor blockade (as in Fig 2). To aid comparison, the data is expressed as% inhibition upon decreasing SR-B1 availability (compared to unblockaded cells). We used the model to predict the outcome of the experiment; in 3.2x CD81 over-expressing cells we expect that complete blockade of SR-B1 inhibits infection by ~50%, compared to ~80% inhibition for unmodified cells. Our experimental data is in good, but not perfect, agreement with the model predictions. Data points represent mean values of n = 4 technical replicates, error bars indicate standard error of the mean. Asterisk indicates a significant difference in inhibition between unmodified and CD81 over-expressing cells (unpaired t-test,GraphPad Prism). Data from one experiment are shown.

https://doi.org/10.1371/journal.pcbi.1006905.g007

upon decreasing SR-B1 availability, i.e. at normal SR-B1 availability infection is uninhibited and is therefore presented as 0% inhibition. Whereas our model predicts that at this level of CD81 overexpression ~70% of viral entry events occur in a SR-B1 independent manner, our experimental data identified a value closer to one half of viral entry occurring in this manner. We note that the mismatch with the novel viral entry data could be resolved if, in line with the sE2 binding data, our original viral entry data supported an increased rate of SR-B1 acquisition relative to the SR-B1 independent rate of gain of CD81. More complex models of viral entry did not resolve this discrepancy between datasets. A model incorporating the unbinding of CD81 receptors by the virus inferred this unbinding to occur at a very low rate, essentially leaving the model unchanged. A model incorporating the unbinding of SR-B1 did not produce a substantial improvement in the model likelihood; we note that the sE2 binding data suggests that SR-B1 is easily acquired and retained (Table 1). As such, while our model is in excellent agreement with the data to which it is fitted, further questions about the behaviour of the system therefore remain.

To summarise, we have used combined experimental and mathematical approaches to provide a number of mechanistic insights into the early processes of HCV entry. Both CD81 and SR-B1 are necessary for efficient entry, however, SR-B1 is somewhat dispensable and a minority of viral particles achieve entry in its absence (Fig 2 and S2 Fig). Soluble E2 binding assays suggest that HCV interactions with SR-B1 are more robust than those with CD81 (Fig 4). We provide a mechanistic model that can be used to understand these observations (Fig 5) and, through mathematical formulation and fitting, demonstrate that is model is consistent with our experimental data (Fig 6). This model was then used to make further predictions about the process of entry, for example providing robust estimates of the proportion of viruses which make the different steps required for viral entry. Our work supports a relatively high stoichiometry of HCV-CD81 interactions during entry with more than ten receptor molecules required for infection (Fig 8).

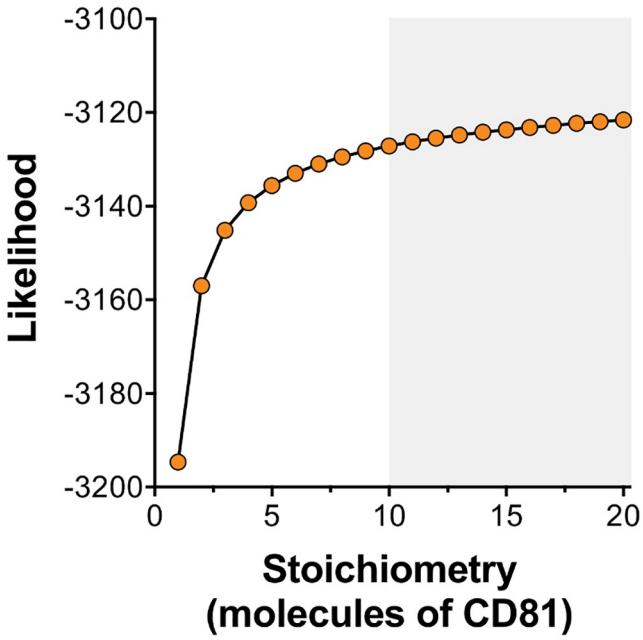

Fig 8. Predicting the stoichiometry of HCV-CD81 interactions. To investigate the number of CD81 molecules that are necessary for HCV entry we performed model optimisation across a range of potential HCV-CD81 stoichiometries. The log likelihood provides a measure of model fit, with higher values indicating a better fit. No peak in likelihood was achieved, however, low stoichiometries are unlikely. The model supports the notion that HCV must achieve a threshold of ~10 CD81 molecules to enter, as highlighted.

https://doi.org/10.1371/journal.pcbi.1006905.g008

Discussion

We have here outlined a novel quantitative model of the early steps of HCV viral entry, based upon newly collected experimental data. By contrast to a previous model of viral entry [28] our approach accounts not only for the role of CD81 receptors in viral entry, but also the influence of SR-B1 receptors upon this process. Our accounting for this interaction is minimally complex, proposing SR-B1-mediated and non-SR-B1-mediated pathways for the acquisition of CD81 receptors, each occurring at different rates. Nevertheless our model produces an extremely good fit to the data to which it is fitted. Our model produced a broad range of potential insights into viral infection. In so far as our model focuses upon viral interactions with CD81 and SR-B1 only, we note that other essential receptors, CLDN1 and OCLDN, are not considered in our model; the 'downstream' stages of entry, which we represent in our model as a single step occurring at an inferred fixed rate, are complex and poorly understood.

Perhaps the clearest result of our model was the insight provided into the successive bottlenecks that block the way to HCV particles achieving infection. In our experiment a very small proportion of viruses associated with the target cells. Having achieved this, only one in three particles completed the acquisition of CD81 receptors, and of those only ~4% of viruses then proceeded to productive infection. This apparent bottleneck is likely due to attritional loss of particles along the entry pathway. Following accumulation of CD81, HCV needs to commandeer at least three other factors (EGFR, claudin-1 and occludin) and complete the process of fusion; inefficiencies and losses at each of these steps will result in a stepwise reduction in particle number. We expect that similar inefficiencies occur *in vivo*, where they are likely to be compounded by the presence of non-permissive target tissues and an active immune response. Together the difficulties in viral entry may contribute to the extreme bottleneck observed for HCV transmission, where infection is established by only 1–5 viral particles [44–46].

While being less precise in this statistic, our model suggests that a multiple CD81 receptors are required for viral entry. A previous mathematical modelling approach inferred that 1–13 E2-CD81 interactions being necessary for HCV entry [28]; our model favoured outcomes at the upper end of this range or above. We note that the two models differ greatly in their evaluation of the acquisition of CD81 receptors. Where the previous model envisaged binding as an effectively instantaneous process between viral proteins and receptors at the interface between the viral and cellular surfaces our approach considers a temporal process involving the stepwise acquisition of receptors.

Our choice of model design, in which HCV achieves viral entry by the stepwise accumulation of receptors, is supported by a broad range of experimental evidence. For example, Baktash et. al. perform single particle tracking of HCV entry in to human hepatoma organoids [38]. This work demonstrates that entry occurs via a two-phase process, in the first of which HCV forms a tripartite receptor complex with SR-B1, CD81 and EGFR at the basolateral cell surface. Numerous other studies have assessed HCV entry kinetics using time of addition inhibitor studies; these experiments suggest that SR-B1 functions immediately after virus attachment, and likely precedes CD81 engagement [12,40,41]. Furthermore, multiple reports have been made of a minority fraction of infection that persists despite targeting of SR-B1 with CRISPR, siRNA or antibody blockade [39,41,47,48], supporting the notion of an SR-B1-independent mode of entry.

A further output from our model was the number of E2 proteins available for binding, suggesting values that are equivalent to the numbers of CD81 receptors required for entry. We note that the number of glycoprotein complexes per HCV particle remains unknown; our estimates of receptor stoichiometry provide a feasible lower bound for the number of functional E2 proteins per virus. This may suggest that unlike related flaviviruses such as Dengue, which possess 180 E proteins per particle, HCV glycoprotein incorporation is low, similar to HIV. This is supported by immunogold EM imaging of isolated HCV particles, which demonstrated limited detection of E2 [49]. Our model also demonstrates an interdependency between SR-B1 and CD81 (Fig 7); such a picture can potentially be used to predict synergies between targeted therapies. For instance when targeted individually our model predicts that a 50% inhibition of infection would require 70–80% of SR-B1/CD81 molecules to be successfully blocked. Whereas, when targeted simultaneously a >50% inhibitory effect can be achieved by blocking 50% of each receptor. This may inform the use of entry inhibitors in combination therapy [16,17].

The key challenge identified by our study, relevant to the estimation of stoichiometry, is the difficulty in quantifying the relative abilities of HCV to acquire SR-B1 or CD81 receptors (c_1 and s in the model). Our experiments evaluating the binding of sE2 binding suggest that E2 binding to SR-B1 is much more robust than to CD81. This finding is supported by previous reports [50] and is consistent with the current structural understanding of E2, which suggests that the SR-B1 binding site (HVR-1) is highly exposed on the surface of E2, whereas the CD81 binding site is likely to be shielded within the tertiary fold of the protein [51–53]. However, numerous technical caveats mean that it is inappropriate to extract a verbatim interpretation of these experiments. Our model of viral entry suggested that the E2-SR-B1 interactions are moderately stronger in magnitude than the E2-CD81, with a two to three-fold difference in propensities. However, both the sE2 data (Fig 4) and SR-B1 blockade in the context of CD81 overexpression (Fig 7) mediate in favour of a greater difference. Under our likelihood framework the sE2 binding data did not have a great influence on the model output; accurate measurements of HCV particle-receptor interactions would likely improve the predictive power of our model.

Further limitations in our model can also be considered. Our model assumes a homogeneity of virus particles and cells, for example ignoring variation in receptor density between cells. On one hand, this assumption may not be too problematic: our experimental data are ensemble measurements derived from a large number of viruses infecting a large number cells, as such, any heterogeneity is likely to be averaged out across these large populations. However, it should be noted that HCV particles are heterogeneous due to their association with host lipoprotein components. Moreover, HCVcc may not fully recapitulate the lipidation status of HCV found circulating in infected humans [31]. To further investigate this it may be necessary to perform parallel experiments characterising the entry of different purified HCV species of varying lipidation status. Whilst this approach may provide valuable information, we decided that it went beyond the scope of this study. We further assume that each of the E2 glycoproteins on a virus particle acts independently, that is to say that receptor binding of one molecule of E2 does not positively or negatively impact the functionality of its neighbours. While this assumption may be problematic, speculation about alternative possibilities is difficult due to the limited information about the arrangement or oligomeric state of glycoproteins on HCV particles.

Our model provides new insight into the HCV entry process, suggesting that initial E2-SR-B1 interactions prime subsequent CD81 interactions. Mechanistically, this is most easily explained through analogy to HIV entry, where primary interactions between Env and CD4 stabilise an alternative conformation of gp120 that is activated for secondary binding to CCR5/CXCR4 [54,55]. This type of mechanism also fits with the presentation of the receptor binding sites on E2: SR-B1 interaction may directly or allosterically result in the unshielding of CD81 binding residues. However, despite ongoing investigations we have yet to gain direct evidence of SR-B1-dependent conformational changes in E2. Alternatively, SR-B1-dependent priming may occur in a less direct manner; for instance, the orientation of a virus particle bound to SR-B1 may promote CD81 binding. Indeed, recent crystallographic studies suggest that CD81 adopts a compact conformation that is likely to project from the plasma membrane by only 1-2nm [56]. In contrast the large ectodomain of SR-B1 is thought to form a barrel like conformation that extends much further from the cell surface [57].

This work provides a template for understanding the molecular interactions of HCV entry and raises a number of pertinent questions for future investigation. For instance, the receptor binding capacity of E2 is likely to vary under viral adaptation, therefore, we may expect different HCV strains to exhibit different entry characteristics. Our modelling approach could be used as an investigative tool to ask important questions in this area, for example: do the entry characteristics of transmitted/founder viruses differ from those circulating in a chronically infected person? Furthermore, our work provides evidence for sequential, interdependent receptor interactions; are these functional stages of virus entry determined by specific conformations of the viral glycoproteins, and if so, which of these conformations is most relevant for B-cell immunogen development?

Methods

Experimental methods

Cell lines. Huh-7.5 cells were provided by APATH LLC; Huh-7 and CRISPR Cas9 receptor KO cells were a gift from Yoshiharu Matsuura (Osaka University) [39]; CHO and HEK 293T cells were acquired from the American Type Culture Collection. All cells were propagated in Dulbecco's Modified Eagle Medium (DMEM) + 10% fetal calf serum (FCS) supplemented with penicillin, streptomycin and non-essential amino acids (Life Technologies, Carlsbad, CA, USA).

Antibodies. Rabbit anti-SR-B1 polyclonal serum was a gift from Thierry Huby (INSERM, Paris); mouse monoclonals anti-CD81 (2.131) and anti-NS5 (S38) were gifts from Jane McKeating (University of Oxford); StrepMAB-Classic was acquired from IBA lifesciences (Göttingen, Germany); anti-LDLR (2148-LD) was purchased from R&D Systems (Minneapolis, MN, USA).

Generation of HCVcc and infection assay. Full-length HCVcc RNA genomes were generated by *in vitro* transcription from J6/JFH plasmid template (provided by APATH LLC) [30,37]. To initiate infection, viral RNA was electroporated into Huh-7.5 cells using a BTX830 (Harvard Instruments, Cambridge, UK). From 3–7 days post electroporation, cell culture supernatants containing infectious J6/JFH HCVcc were harvested every 2–4 h; these short harvest times limit the opportunity for virus degradation, therefore, preventing the accumulation of non-infectious particles. A uniform experimental stock of virus was generated by pooling the harvested supernatants; this ensures maximum reproducibility between experiments.

To assess HCVcc infectivity Huh-7.5 cells were seeded at a density of 1.5×10^4 in to each well of a standard flat bottomed 96-well tissue culture test plate 24 h prior to study. Receptor availability was modulated as described below. To infect, the cells were refed with 50μl of DMEM + 3% FCS and challenged with an equal volume of HCVcc supernatants diluted 1/2 in DMEM + 3% FCS (this resulted in each well receiving ~180 foci forming units of infectious virus). After 5 h the inoculum was removed, and the cells were washed twice in 50 μL PBS and refed with 100μl DMEM 3% FCS. Cells were fixed after 48 hours by washing with 50μl of PBS and treatment with 250μl ice cold methanol for 10 min, at this time point only one round of infection is apparent. To detect viral antigen, samples were blocked with 0.5% bovine serum albumin (BSA) stained with anti-NS5 (S38) hybridoma supernatant (1/100), followed by 2 μg/mL goat anti-mouse Alexa Fluor 647 secondary antibody (Life Technologies). Nuclear DNA was counterstained with 2 μg/mL 4′,6-diamidino-2-phenylindole (DAPI).

To quantify infection assay plates were imaged using a Nikon Ti inverted microscope fitted with a motorized encoded stage for plate-reading. A 4 mm by 4 mm area of each well was acquired by image stitching using an ORCA Flash 4 sCMOS camera (Hamamatsu, Welwyn Garden City, UK), with 405 nm and 647 nm fluorescence illumination provided by a PE4000 LED unit (CoolLED, Andover, UK) through a multi-band excitation/emission filter cube (Semrock, Rochester, NY, US). To ensure optimal imaging, software-based autofocusing was performed prior to acquiring each well. The number of foci in each image was quantified manually using the counting tool in FIJI/ImageJ [58,59]. In addition, the number of DAPI nuclei were counted using the 'find maxima' function, this data was later used to derive estimates of the probability of infection (described below).

Antibody-mediated receptor blockade. To limit the availability of receptor, Huh-7.5 cells seeded for infection were pre-incubated at 37˚C with 50μl of media containing a serial dilution of either rabbit anti-SR-B1 polyclonal serum [37] or mouse anti-CD81 (2.131) hybridoma supernatant [36]. After 45 mins, the wells were challenged with virus, as described above.

Lentivirus-mediated over-expression. To generate lentiviral vectors we transfected HEK 293T cells with three plasmids: a HIV packaging construct (pCMV-dR8.91), VSV-G envelope plasmid (pMD2.G) and a dual promoter transfer plasmid encoding GFP in combination with SR-B1 or CD81 (pDual SR-B1 or CD81, available from Addgene). Huh-7.5 cells were transduced with lentivirus vectors, diluted in DMEM + 10% FCS, 96 hours before an experiment; 24 hours prior to study the cells were seeded into a 96 well plate for infection, as described above.

Quantification of receptor availability. In parallel with the infection assay we also prepared plates to assess receptor availability. Pre-treatment of these plates was identical to those being infected, however, instead of receiving virus they were mock inoculated with

DMEM + 3% FCS. After 5 hours the plates were then washed once with PBS and fixed with 4% formaldehyde. The plates were then blocked for 1 hour in 0.5% BSA before staining to assess receptor modulation. To evaluate antibody-mediated receptor blockade, bound antibody was detected by addition of goat anti-mouse/rabbit Alexa Fluor 647 secondary antibody. To evaluate receptor over-expression, fixed cells were incubated with a saturating concentration of anti-SR-B1 or CD81 followed by anti-mouse/rabbit Alexa Fluor 647 secondary antibody. Nuclear DNA was counterstained with 2 μg/mL DAPI. Imaging was performed as described above and image analysis/quantification was performed in FIJI/ImageJ.

Quantification of viral copy number by qPCR. Virus particle attachment was assessed by qPCR quantification of cell-associated RNA genome copy numbers. Cells were seeded and inoculated as described above for the infection assay, however, after 5 hours the cells were washed 3 times in PBS and then lysed for viral RNA extraction using a QIAamp Viral RNA Mini Kit (Qiagen, Hilden, Germany). RNA quantification was performed using a Luna Universal qRT-PCR kit (New England Biolabs, Ipswich, MA, USA) with primers targeting the 5' UTR of the HCV genome (sense primer: GCGAAAGGCCTTGTGGTACT, anti-sense primer: CACGGTCTACGAGACCTCCC) as previously described [60]. RNA copy number was determined by including a standard curve of in vitro transcribed HCV RNA in each qPCR run. Reactions were run on a CFX96 touch thermal cycler (Bio-Rad, Hercules, CA, USA).

Soluble E2 binding assay. A truncated, soluble version of the E2 glycoprotein (sE2) was cloned by PCR amplification from a plasmid encoding full length HCV genome and ligated into a vector encoding an N-terminal tPA secretion signal and a C-terminal Twin-Strep-Tag [61,62]. sE2 was produced by transient transfection of HEK 293T cells followed by protein purification using the Step-TactinXT system (IBA lifesciences, Göttingen, Germany). To assess E2 interaction with receptors, CHO cells were transduced with lentivirus encoding human SR-B1 or CD81, transgene expression was allowed for at least 72 hours before the cells were used in a sE2 binding assay, as previously described [62]. Briefly, cells were trypsinised into a single cell suspension, and then incubated in blocking buffer (1% BSA + 0.01% NaN_3) for 20 minutes, note that the inclusion of NaN_3 stops cellular metabolism and arrests internalisation of surface bound ligands. sE2, diluted in blocking buffer, was incubated with the cells for 1 hour at 37˚C, followed by two PBS washes. Bound E2 was detected using anti-Strep-Tag antibody and goat anti-mouse Alexa Fluor 647 secondary antibody. Samples were quantified on a LSR-Fortessa cell analyser and the data anlysed using FlowJo (both Becton Dickinson, Franklin Lakes, NJ, USA).

Computational methods

Multiple independent receptor blockade and over-expression studies were performed, as illustrated in Figs 2 and 3. These, along with the quantification of particle attachment (Fig 1), provide the necessary information to estimate the effect of receptor availability on the probability of infection; this data can then be used to fit our model. Achieving these estimates required some analysis and processing of the raw data.

Processing of fluorescence data. The use of fluorescence data to quantify the number of receptors available for binding poses two challenges. Firstly, measurements of fluorescence are imprecise, with an unknown level of variance in a repeat measurement. Secondly, measurements collected from different cell populations may not give consistent results; the level of fluorescence indicating saturation may vary from one population to another. Measurements were therefore processed to produce normalised estimates of how many receptors were available in each population.

Firstly, to account for imprecision in fluorescence measurements, we clustered data from populations which had been titrated with different quantities of antibody, identifying sets of readings which could be meaningfully distinguished from each other. For each set of cells i having a constant antibody concentration we denote the fluorescence values collected as $\{f_i\}$. Sorting each set of values, we carried out a two-sample T-test on all pairs of differing sets $\{f_i\}$ and $\{f_j\}$, identifying the pair of sets for which the test produced the highest p-value. If this p-value was greater than 0.05, indicating that the two sets of values could not be clearly statistically separated, the two sets were merged, repeating the calculation of T-tests across the new pairs of sets. Where sets contained different numbers of fluorescence values, 100 random samples were drawn from the larger set, each of size equal to that of the smaller set, and the mean p-value across these samples was calculated. Examples of mean and standard deviations of fluorescence values from distinct antibody concentrations taken before and after this clustering procedure are shown in S9 Fig, this relates to the raw data shown in Fig 2.

Secondly, clustered fluorescence data were normalised to estimate the proportion of receptor available in each set following the addition of antibody. For each set, the maximum fluorescence, denoted max f, was calculated as the mean of the fluorescence values from the cells with the highest amount of antibody; this was assumed to indicate saturation of receptors. Similarly, the minimum fluorescence, denoted min f, was calculated as the mean of the fluorescence values from the cells for which no antibody was added. For the set $\{f_i\}$, the proportion of receptors available was then calculated as

$$\frac{1}{n}\sum_{k=1}^{n}\left(\frac{f_{ik}-\max f}{\min f-\max f}\right)$$

Processing of cell count data. Within the experiment, measurements of the total number of cells in each well were collected after 5 and 48 hours (S1 Fig). These values were compared in order to account for the growth of cells during the experiment. This ratio was then used to scale the 48-hour cell counts, producing estimated 6-hour cell counts, corresponding to the number of cells in a well at the time of viral infection. We denote these estimated number of cells for a given population as a_i.

Viral inoculum dose. An estimation of the effective viral dose for each set of cells was calculated. Attachment to the cell membrane is an essential precursor to viral entry. In measuring viral entry our concern is for events subsequent to this attachment. As such, rather than considering the pure ratio of number of viruses to number of cells in a well, we evaluated the mean number of viruses attaching to the cell membrane of each cell.

For a replicate set of cells, a large number of viruses was added to each well, following which the number of viruses bound to the membrane after 5 hours was calculated (Fig 1). This suggested that a mean of $n = 11125$ viruses were bound to the cell membrane. Cell counts were made using images which covered a 4mm^2 portion of each well, equivalent to a fraction of 0.454 of the well area. As such, the effective dose was calculated as

$$m = \frac{0.454n}{\bar{a}_i} \approx 0.767 \text{ viruses per cell}$$

where the bar indicates a mean value across all populations. The dose was assumed to remain constant across all wells, assuming that small changes in the number of cells would be reflected by corresponding changes in the number of membrane-attached viruses.

Likelihood model for viral entry. Given an a viral inoculum dose, the expected fraction q_k of cells in each well that are infected by k viruses, was modelled using a Poisson distribution:

$$q_k = \frac{m^k e^{-m}}{k!}$$

We developed a deterministic model, described below, to estimate the probability P_i that a virus which is bound to the cell membrane in well i gains viral entry. Supposing that viruses act independently of one another in gaining entry to a cell, the probability that at least one virus gains entry to a cell to which k viruses are bound is given by $1\text{-}(1\text{-}P_i)^k$. Given counts o_i of the number of foci of infection in each population, we then used a double Poisson model to calculate the likelihood of a model:

$$\log L_1 = \log\left[\theta^{0.5} e\theta\mu \left(\frac{e^{-o_i} o_i^{o_i}}{o_i!}\right)\left(\frac{e\mu}{o_i}\right)^{\theta o_i} C\right]$$

Where

$$\frac{1}{C} = 1 + \left(\frac{1-\theta}{12\theta\mu}\right)\left(1 + \frac{1}{\theta\mu}\right)$$

This model, while superficially similar to a Poisson model, grants additional flexibility, the variance of the distribution being controlled by the parameter θ. This parameter was estimated using a likelihood model to fit a probability P_i to data from each set of wells defined by the fluorescence data, without these probabilities being constrained by any underlying model. This gave the estimated value $\theta \approx 0.363$, representing an increased variance in the data relative to a Poisson distribution.

Data from the sE2 experiments were used to characterise the ratio between the intrinsic binding of the virus to CD81 and SR-B1 receptors. A gamma distribution with parameters α and β was fitted to data describing the ratio between the extent of viruses bound at saturation, giving the likelihood

$$\log L_2 = \frac{1}{\Gamma(\alpha)\beta} x^{\alpha-1} e^{-x/\beta}$$

where $x = s/c_1$ is the ratio between the intrinsic rates of binding CD81 and SR-B1 in our model.

The total likelihood for our model was then calculated as

$$\log L = \log L_1 + \log L_2$$

Processing of overexpression data. Data were collected both from populations of cells grown with antibody to reduce the number of available receptors, and for populations of cells in which the over-expression of receptors was induced. To account for potential differences in cell populations, a linear scaling was applied to produce identical results for wild-type cells. Inferred frequencies from the estimation of θ were used to scale the parameters a_i in the over-expression data to produce identical estimates of P_i for each equivalent set of wild-type cells; our model therefore assessed how changes in receptor availability lead to changes in viral entry.

Intra-cellular model of infection. In the framework above we require an estimate for the value P, describing the probability that a single virus that binds to the cell membrane gains entry to the cell. To calculate this value we use an ODE model of viral dynamics (Fig 5B) to

estimate this. As described in the main text, our model contains the parameters r, describing the number of CD81 receptors required to gain entry into the cell, e, the downstream rate of viral entry having bound sufficient CD81 receptor, s, the rate at which viruses acquire SR-B1 receptors, c_1 and c_2, describing SR-B1-independent and SR-B1-mediated rates of acquiring CD81 receptors, N_e, the number of available E2 proteins in a virus, plus a 'death rate' for viruses, d. Mathematically, we consider the behaviour of viruses which are associated with the membrane. We denote the proportion of viruses to have gained viral entry by E, and the proportion of viruses which have died by D. We denote the proportion of viruses in which i E2 have bound to CD81 receptors and in which j of the remaining E2 have associated with SR-B1 receptors as $M_{i,j}$.

Our model can then be described mathematically as:

$$\frac{dD}{dt} = d\sum_{ij} M_{i,j}$$

$$\frac{dE}{dt} = e\sum_{j=r} M_{i,j}$$

$$\begin{aligned}\frac{dM_{i,j}}{dt} &= \frac{1}{N_e}[p_c(c_1(N_e-i-j+1)M_{i-1,j}+c_2jM_{i-1,j+1})+p_s(s(N_e-i-j+1)M_{i,j-1})]\\ &\quad -\frac{1}{N_e}[(p_c(c_1(N_e-i-j)+c_2j)+p_s(N_e-i-j))M_{i,j}]-dM_{i,j} \text{ if } i<r\end{aligned}$$

$$\begin{aligned}\frac{dM_{i,j}}{dt} &= \frac{1}{N_e}[p_c(c_1(N_e-i-j+1)M_{i-1,j}+c_2jM_{i-1,j+1})+p_s(s(N_e-i-j+1)M_{i,j-1})])\\ &\quad -\frac{1}{N_e}[(p_c(c_1(N_e-i-j)+c_2j)+p_s(N_e-i-j))M_{i,j}]-dM_{i,j}-eM_{i,j} \text{ if } i = r\end{aligned}$$

where for convenience $M_{i,j}$ is defined as being zero for all i and j outside of the ranges $0 \leq i \leq r$ and $0 \leq j \leq N_e$ and in which the system has the initial conditions $D = 0$, $E = 0$, $M_{0,0} = 1$, and $M_{i,j} = 0$ for all $i > 0$ and $j > 0$.

Simulations were run using a fourth-order Runge-Kutta scheme with an adaptive step size until the sum of the terms D+E was greater than 0.999. At this point, we calculated the value

$$P(\text{virus gains entry}) = \frac{E}{D+E}$$

Thus obtaining the proportion of viruses to have gained entry into the cell. The death rate d was arbitrarily fixed to the value 0.01, all other rates being calculated relative to this. Likelihood values were compared for models in which different numbers of CD81 receptors were required for entry, specified by the parameter r.

Statistics of viral entry. Among the viruses which acquire sufficient CD81 receptors, not all go on to gain entry to the cell. The proportion of viruses which do gain entry can be simply inferred from the model parameters; having acquired sufficient receptors, virus particles gain viral entry at rate e, and die at rate d. The proportion of viruses with sufficient CD81 receptors which gain viral entry is therefore given by

$$P(\text{virus gains entry}|\text{virus gains sufficient CD81}) = \frac{e}{d+e}$$

From this statistic we can derive the number of viruses which gain sufficient CD81 receptors

to be able to potentially gain viral entry, as

$$P(\text{virus gains sufficient CD81}) = \frac{P(\text{virus gains entry})}{(\text{virus gains entry}|\text{virus gains sufficient CD81})}$$

Alternative models. The model described above contains a number of choices in the potential biological effects included or excluded from the model. Other models were considered, for example incorporating the unbinding of the CD81 and SR-B1 receptors; details are given in S1 Text.

Supporting information

S1 Fig. Infection assay workflow and quantification. A. The infection assay workflow: cells were manipulated to achieve receptor blockade or over-expression at the indicated time points. Plate 1 was used to determine HCV infectivity, whereas the parallel plate 2 was used to assess receptor blockade/over expression. **B**. Infection was quantified manually by counting infected foci at 48 hours. At this time point only one round of infection is apparent. i. An example field of HCV infected Huh-7.5 cells stained for viral antigen and cellular nuclei. ii. A large image of the inset from A., multiple distinct foci of infection are apparent. iii. Viral infection was quantified by manual scoring of individual foci, as annotated on to the image. Scale bar 200μm.
(TIF)

S2 Fig. HCV challenge of receptor KO cells confirms SR-B1 independent infection. HCV titre in parental Huh-7 human hepatoma cells, or those in which receptor encoding genes have been knocked out by CRISPR Cas9 editing. Mean values of n = 3 independent experiments are shown. Error bars indicate standard error of the mean. Asterisk indicates a significant difference between SR-B1 KO and parental Huh-7 cells (unpaired t-test, GraphPad Prism).
(TIF)

S3 Fig. Lentiviral transduction of Huh-7.5 cells is homogenous. Huh-7.5 cells were transduced with lentiviral vectors that encode both a receptor (either SR-B1 or CD81) and GFP, expressed from separate promoters. Therefore, evaluating GFP expression provides an independent measure of transduction efficiency. The images display representative fluorescent micrographs of parental cells or those transduced with SR-B1 + GFP lentiviral vectors. GFP expression is homogenous between cells and titrates with lentivirus concentration.
(TIF)

S4 Fig. Transduced CHO cells express exogenous SR-B1/CD81. CHO cells were transduced with lentivirus encoding either SR-B1 or CD81 and GFP (as described in S3 Fig), receptor expression was assessed by flow cytometry. **A**. Representative dot plots of receptor and GFP expression in CHO cells, unlike Huh-7.5 cells, a minority of cells remained GFP/receptor negative. **B**. Representative histograms of receptor expression in GFP negative and positive CHO cells, as expected, receptor expression is only apparent in GFP positive cells.
(TIF)

S5 Fig. Representative raw data of sE2 binding to CHO SR-B1/CD81 cells. Representative median fluorescence intensity values for sE2 binding to CHO SR-B1/CD81 cells, as assessed by flow cytometry. Background is determined by sE2 binding to untransduced CHO cells. Data points represent the mean of n = 2 technical repeats. Error bars indicate standard error of the mean. Data was fitted using a one-site binding curve in GraphPad Prism.
(TIF)

S6 Fig. Soluble E2 binding to CHO cells expressing CD81 is low but readily detectable. Representative raw data showing sE2 binding to CHO cells transduced with lentiviral vectors encoding CD81 + GFP. **A**. Dot plots displaying sE2 binding and GFP expression in untreated CHO-CD81 cells and those incubated with 40μg/ml sE2. **B**. sE2 binding to GFP negative and positive cells within the same sample, as expected, sE2 binding is only detectable in GFP positive cells, i.e those that have been successfully transduced with receptor encoding lentivirus.
(TIF)

S7 Fig. The likely ratio between E2-SR-B1 and E2-CD81 binding. Data from the sE2 binding experiments (Fig 4) were used to characterise the ratio between the intrinsic binding of the virus to CD81 and SR-B1 receptors. A gamma distribution with parameters α and β, was fitted to data describing the ratio between the extent of viruses bound at saturation. Peak likelihood was achieved at a ratio of ~20. Asterisks indicate the experimentally measured ratio from 5 independent experiments.
(TIF)

S8 Fig. LDLR is unlikely to mediate SR-B1 independent entry. A. A report by Yamamoto et. al. suggests redundancy between SR-B1 and LDLR. Therefore we investigated the possibility that LDLR functions in an analogous manner to SR-B1, as illustrated. Note the molecular model of LDLR is based on a partial crystal structure (PDB: 3P5C [65]); full length LDLR is likely to be significantly longer than represented here. **B**. Antibody mediated receptor blockade of SR-B1 and LDLR inhibit HCVcc infection. **C**. Titre of HCVcc in Huh-7 cells gene-edited to remove SR-B1 and LDLR, data is expressed as a percentage of parental cells. Both gene edited cell lines display a statistically significant reduction in titre when compared to parental cells, and to each other, as denoted by asterisks. **D**. Example raw infection data upon combination of anti-SR-B1 and anti-LDLR. SR-B1 blockade does not increase the inhibitory activity of anti-LDLR, as annotated on the plot. **E**. Inhibition of HCV infection by anti-LDLR upon increasing concentration of anti-SR-B1, we measured no significant difference between treatments. This lack of synergy suggests that the model presented in A is incorrect; LDLR does not mediate SR-B1-independent entry. All data points are mean values of n = 3 independent repeats, apart from D., which displays raw data. Error bars indicate standard error of the mean. Significance testing performed using an unpaired t-test (GraphPad Prism).
(TIF)

S9 Fig. Clustering and processing of fluorescence data. We estimated receptor availability from fluorescence microscopy data. **A**. Representative raw fluorescence measurements of anti-SR-B1/CD81 binding to Huh-7.5 cells (similar to Fig 2A), data points represent the mean of n>4 technical repeats, error bars indicate standard deviation of the mean. **B**. Statistically indistinguishable data points were clustered together and averaged; the clustered measurements and their resulting combined data point are annotated. **C**. Scaled estimates of receptor availability derived from clustered data. Maximum antibody binding indicates saturation of receptor and, therefore, availability = 0; whereas in untreated cells receptor availability is set to 1. These receptor availability values can then be compared to matched infection data to explore HCV receptor availability. In each plot data was fitted using a sigmoidal curve in GraphPad Prism.
(TIF)

S1 Table. Comparison of inferred parameters from the complete dataset and from a reduced dataset in which the sE2 binding data were omitted. While the sE2 data constrain the ratio between the parameters s and c_1, this had very little impact on the final optimised values.
(DOCX)

S1 Text. Mathematical description of alternative models for viral entry. We describe a null model, in which SR-B1 has no effect on viral entry, and models with additional parameters describing the loss of CD81 and SR-B1 receptors.
(DOCX)

S1 Data. Data accompanying figures.
(XLSX)

Author Contributions

Conceptualization: Joe Grove, Christopher J. R. Illingworth.

Data curation: Joe Grove, Christopher J. R. Illingworth.

Formal analysis: Dilyana Mincheva, Christopher J. R. Illingworth.

Funding acquisition: Joe Grove, Christopher J. R. Illingworth.

Investigation: Mphatso Kalemera, Dilyana Mincheva, Joe Grove, Christopher J. R. Illingworth.

Methodology: Mphatso Kalemera, Dilyana Mincheva, Joe Grove, Christopher J. R. Illingworth.

Project administration: Joe Grove, Christopher J. R. Illingworth.

Resources: Joe Grove, Christopher J. R. Illingworth.

Software: Dilyana Mincheva, Christopher J. R. Illingworth.

Supervision: Joe Grove, Christopher J. R. Illingworth.

Validation: Joe Grove, Christopher J. R. Illingworth.

Visualization: Joe Grove, Christopher J. R. Illingworth.

Writing – original draft: Joe Grove, Christopher J. R. Illingworth.

Writing – review & editing: Mphatso Kalemera, Dilyana Mincheva, Joe Grove, Christopher J. R. Illingworth.

References

1. Stanaway JD, Flaxman AD, Naghavi M, Fitzmaurice C, Vos T, Abubakar I, et al. The global burden of viral hepatitis from 1990 to 2013: findings from the Global Burden of Disease Study 2013. Lancet. 2016; 388: 1081–1088. https://doi.org/10.1016/S0140-6736(16)30579-7 PMID: 27394647
2. Scheel TKH, Rice CM. Understanding the hepatitis C virus life cycle paves the way for highly effective therapies. Nat Med. 2013; 19: 837–849. https://doi.org/10.1038/nm.3248 PMID: 23836234
3. Liang TJ, Jake Liang T, Ward JW. Hepatitis C in Injection-Drug Users—A Hidden Danger of the Opioid Epidemic. N Engl J Med. 2018; 378: 1169–1171. https://doi.org/10.1056/NEJMp1716871 PMID: 29601263
4. Ding Q, von Schaewen M, Ploss A. The impact of hepatitis C virus entry on viral tropism. Cell Host Microbe. 2014; 16: 562–568. https://doi.org/10.1016/j.chom.2014.10.009 PMID: 25525789
5. Pileri P. Binding of Hepatitis C Virus to CD81. Science. 1998; 282: 938–941. PMID: 9794763
6. Scarselli E, Ansuini H, Cerino R, Roccasecca RM, Acali S, Filocamo G, et al. The human scavenger receptor class B type I is a novel candidate receptor for the hepatitis C virus. EMBO J. 2002; 21: 5017–5025. https://doi.org/10.1093/emboj/cdf529 PMID: 12356718
7. Evans MJ, von Hahn T, Tscherne DM, Syder AJ, Panis M, Wölk B, et al. Claudin-1 is a hepatitis C virus co-receptor required for a late step in entry. Nature. 2007; 446: 801–805. https://doi.org/10.1038/nature05654 PMID: 17325668

8. Ploss A, Evans MJ, Gaysinskaya VA, Panis M, You H, de Jong YP, et al. Human occludin is a hepatitis C virus entry factor required for infection of mouse cells. Nature. 2009; 457: 882–886. https://doi.org/10.1038/nature07684 PMID: 19182773
9. Lupberger J, Zeisel MB, Xiao F, Thumann C, Fofana I, Zona L, et al. EGFR and EphA2 are host factors for hepatitis C virus entry and possible targets for antiviral therapy. Nat Med. 2011; 17: 589–595. https://doi.org/10.1038/nm.2341 PMID: 21516087
10. Voisset C, Callens N, Blanchard E, Op De Beeck A, Dubuisson J, Vu-Dac N. High Density Lipoproteins Facilitate Hepatitis C Virus Entry through the Scavenger Receptor Class B Type I. J Biol Chem. 2005; 280: 7793–7799. https://doi.org/10.1074/jbc.M411600200 PMID: 15632171
11. Kong L, Giang E, Nieusma T, Kadam RU, Cogburn KE, Hua Y, et al. Hepatitis C virus E2 envelope glycoprotein core structure. Science. 2013; 342: 1090–1094. https://doi.org/10.1126/science.1243876 PMID: 24288331
12. Mankowski MC, Kinchen VJ, Wasilewski LN, Flyak AI, Ray SC, Crowe JE Jr, et al. Synergistic anti-HCV broadly neutralizing human monoclonal antibodies with independent mechanisms. Proc Natl Acad Sci U S A. 2018; 115: E82–E91. https://doi.org/10.1073/pnas.1718441115 PMID: 29255018
13. von Hahn T, Yoon JC, Alter H, Rice CM, Rehermann B, Balfe P, et al. Hepatitis C virus continuously escapes from neutralizing antibody and T-cell responses during chronic infection in vivo. Gastroenterology. 2007; 132: 667–678. https://doi.org/10.1053/j.gastro.2006.12.008 PMID: 17258731
14. Ball JK, Tarr AW, McKeating JA. The past, present and future of neutralizing antibodies for hepatitis C virus. Antiviral Res. 2014; 105: 100–111. https://doi.org/10.1016/j.antiviral.2014.02.013 PMID: 24583033
15. Giang E, Dorner M, Prentoe JC, Dreux M, Evans MJ, Bukh J, et al. Human broadly neutralizing antibodies to the envelope glycoprotein complex of hepatitis C virus. Proc Natl Acad Sci U S A. 2012; 109: 6205–6210. https://doi.org/10.1073/pnas.1114927109 PMID: 22492964
16. Padmanabhan P, Dixit NM. Inhibitors of hepatitis C virus entry may be potent ingredients of optimal drug combinations. Proc Natl Acad Sci U S A. 2017; 114: E4524–E4526. https://doi.org/10.1073/pnas.1704531114 PMID: 28512229
17. Ohashi H, Koizumi Y, Fukano K, Wakita T, Perelson AS, Iwami S, et al. Reply to Padmanabhan and Dixit: Hepatitis C virus entry inhibitors for optimally boosting direct-acting antiviral-based treatments. Proc Natl Acad Sci U S A. 2017; 114: E4527–E4529. https://doi.org/10.1073/pnas.1705234114 PMID: 28512226
18. Grove J, Marsh M. The cell biology of receptor-mediated virus entry. J Cell Biol. 2011; 195: 1071–1082. https://doi.org/10.1083/jcb.201108131 PMID: 22123832
19. Guedj J, Dahari H, Rong L, Sansone ND, Nettles RE, Cotler SJ, et al. Modeling shows that the NS5A inhibitor daclatasvir has two modes of action and yields a shorter estimate of the hepatitis C virus half-life. Proc Natl Acad Sci U S A. 2013; 110: 3991–3996. https://doi.org/10.1073/pnas.1203110110 PMID: 23431163
20. Shirasago Y, Fukazawa H, Aizaki H, Suzuki T, Suzuki T, Sugiyama K, et al. Thermostable hepatitis C virus JFH1-derived variant isolated by adaptation to Huh7.5.1 cells. J Gen Virol. 2018; 99: 1407–1417. https://doi.org/10.1099/jgv.0.001117 PMID: 30045785
21. Graw F, Perelson AS. Modeling Viral Spread. Annu Rev Virol. 2016; 3: 555–572. https://doi.org/10.1146/annurev-virology-110615-042249 PMID: 27618637
22. Gray ER, Illingworth CJR, Coffin JM, Stoye JP. Binding of more than one Tva800 molecule is required for ASLV-A entry. Retrovirology. 2011; 8: 96. https://doi.org/10.1186/1742-4690-8-96 PMID: 22099981
23. Ribeiro RM, Li H, Wang S, Stoddard MB, Learn GH, Korber BT, et al. Quantifying the diversification of hepatitis C virus (HCV) during primary infection: estimates of the in vivo mutation rate. PLoS Pathog. 2012; 8: e1002881. https://doi.org/10.1371/journal.ppat.1002881 PMID: 22927817
24. Graw F, Balagopal A, Kandathil AJ, Ray SC, Thomas DL, Ribeiro RM, et al. Inferring viral dynamics in chronically HCV infected patients from the spatial distribution of infected hepatocytes. PLoS Comput Biol. 2014; 10: e1003934. https://doi.org/10.1371/journal.pcbi.1003934 PMID: 25393308
25. Neumann AU. Hepatitis C Viral Dynamics in Vivo and the Antiviral Efficacy of Interferon- Therapy. Science. 1998; 282: 103–107. PMID: 9756471
26. Dixit NM, Layden-Almer JE, Layden TJ, Perelson AS. Modelling how ribavirin improves interferon response rates in hepatitis C virus infection. Nature. 2004; 432: 922–924. https://doi.org/10.1038/nature03153 PMID: 15602565
27. Guedj J, Pang PS, Denning J, Rodriguez-Torres M, Lawitz E, Symonds W, et al. Analysis of the hepatitis C viral kinetics during administration of two nucleotide analogues: sofosbuvir (GS-7977) and GS-0938. Antivir Ther. 2014; 19: 211–220. https://doi.org/10.3851/IMP2733 PMID: 24464551

28. Padmanabhan P, Dixit NM. Mathematical model of viral kinetics in vitro estimates the number of E2-CD81 complexes necessary for hepatitis C virus entry. PLoS Comput Biol. 2011; 7: e1002307. https://doi.org/10.1371/journal.pcbi.1002307 PMID: 22174670

29. Padmanabhan P, Dixit NM. Viral kinetics suggests a reconciliation of the disparate observations of the modulation of claudin-1 expression on cells exposed to hepatitis C virus. PLoS One. 2012; 7: e36107. https://doi.org/10.1371/journal.pone.0036107 PMID: 22545157

30. Lindenbach BD, Evans MJ, Syder AJ, Wölk B, Tellinghuisen TL, Liu CC, et al. Complete replication of hepatitis C virus in cell culture. Science. 2005; 309: 623–626. https://doi.org/10.1126/science.1114016 PMID: 15947137

31. Lindenbach BD, Meuleman P, Ploss A, Vanwolleghem T, Syder AJ, McKeating JA, et al. Cell culture-grown hepatitis C virus is infectious in vivo and can be recultured in vitro. Proc Natl Acad Sci U S A. 2006; 103: 3805–3809. https://doi.org/10.1073/pnas.0511218103 PMID: 16484368

32. Barth H, Schafer C, Adah MI, Zhang F, Linhardt RJ, Toyoda H, et al. Cellular binding of hepatitis C virus envelope glycoprotein E2 requires cell surface heparan sulfate. J Biol Chem. 2003; 278: 41003–41012. https://doi.org/10.1074/jbc.M302267200 PMID: 12867431

33. Koutsoudakis G, Kaul A, Steinmann E, Kallis S, Lohmann V, Pietschmann T, et al. Characterization of the early steps of hepatitis C virus infection by using luciferase reporter viruses. J Virol. 2006; 80: 5308–5320. https://doi.org/10.1128/JVI.02460-05 PMID: 16699011

34. Fan H, Qiao L, Kang K-D, Fan J, Wei W, Luo G. Attachment and Postattachment Receptors Important for Hepatitis C Virus Infection and Cell-to-Cell Transmission. J Virol. 2017;91. https://doi.org/10.1128/JVI.00280-17 PMID: 28404852

35. Klasse PJ. Molecular determinants of the ratio of inert to infectious virus particles. Prog Mol Biol Transl Sci. 2015; 129: 285–326. https://doi.org/10.1016/bs.pmbts.2014.10.012 PMID: 25595808

36. Grove J, Hu K, Farquhar MJ, Goodall M, Walker L, Jamshad M, et al. A new panel of epitope mapped monoclonal antibodies recognising the prototypical tetraspanin CD81. Wellcome Open Res. 2017; 2: 82. https://doi.org/10.12688/wellcomeopenres.12058.1 PMID: 29090272

37. Grove J, Huby T, Stamataki Z, Vanwolleghem T, Meuleman P, Farquhar M, et al. Scavenger receptor BI and BII expression levels modulate hepatitis C virus infectivity. J Virol. 2007; 81: 3162–3169. https://doi.org/10.1128/JVI.02356-06 PMID: 17215280

38. Baktash Y, Madhav A, Coller KE, Randall G. Single Particle Imaging of Polarized Hepatoma Organoids upon Hepatitis C Virus Infection Reveals an Ordered and Sequential Entry Process. Cell Host Microbe. 2018; 23: 382–394.e5. https://doi.org/10.1016/j.chom.2018.02.005 PMID: 29544098

39. Yamamoto S, Fukuhara T, Ono C, Uemura K, Kawachi Y, Shiokawa M, et al. Lipoprotein Receptors Redundantly Participate in Entry of Hepatitis C Virus. PLoS Pathog. 2016; 12: e1005610. https://doi.org/10.1371/journal.ppat.1005610 PMID: 27152966

40. Zeisel MB, Koutsoudakis G, Schnober EK, Haberstroh A, Blum HE, Cosset F-L, et al. Scavenger receptor class B type I is a key host factor for hepatitis C virus infection required for an entry step closely linked to CD81. Hepatology. 2007; 46: 1722–1731. https://doi.org/10.1002/hep.21994 PMID: 18000990

41. Zahid MN, Turek M, Xiao F, Thi VLD, Guérin M, Fofana I, et al. The postbinding activity of scavenger receptor class B type I mediates initiation of hepatitis C virus infection and viral dissemination. Hepatology. 2013; 57: 492–504. https://doi.org/10.1002/hep.26097 PMID: 23081796

42. Dao Thi VL, Granier C, Zeisel MB, Guérin M, Mancip J, Granio O, et al. Characterization of hepatitis C virus particle subpopulations reveals multiple usage of the scavenger receptor BI for entry steps. J Biol Chem. 2012; 287: 31242–31257. https://doi.org/10.1074/jbc.M112.365924 PMID: 22767607

43. Koutsoudakis G, Herrmann E, Kallis S, Bartenschlager R, Pietschmann T. The level of CD81 cell surface expression is a key determinant for productive entry of hepatitis C virus into host cells. J Virol. 2007; 81: 588–598. https://doi.org/10.1128/JVI.01534-06 PMID: 17079281

44. Stoddard MB, Li H, Wang S, Saeed M, Andrus L, Ding W, et al. Identification, molecular cloning, and analysis of full-length hepatitis C virus transmitted/founder genotypes 1, 3, and 4. MBio. 2015; 6: e02518. https://doi.org/10.1128/mBio.02518-14 PMID: 25714714

45. Wang GP, Sherrill-Mix SA, Chang K-M, Quince C, Bushman FD. Hepatitis C virus transmission bottlenecks analyzed by deep sequencing. J Virol. 2010; 84: 6218–6228. https://doi.org/10.1128/JVI.02271-09 PMID: 20375170

46. Li H, Stoddard MB, Wang S, Blair LM, Giorgi EE, Parrish EH, et al. Elucidation of hepatitis C virus transmission and early diversification by single genome sequencing. PLoS Pathog. 2012; 8: e1002880. https://doi.org/10.1371/journal.ppat.1002880 PMID: 22927816

47. Prentoe J, Serre SBN, Ramirez S, Nicosia A, Gottwein JM, Bukh J. Hypervariable Region 1 Deletion and Required Adaptive Envelope Mutations Confer Decreased Dependency on Scavenger Receptor

Class B Type I and Low-Density Lipoprotein Receptor for Hepatitis C Virus. J Virol. 2013; 88: 1725–1739. https://doi.org/10.1128/JVI.02017-13 PMID: 24257605

48. Zuiani A, Chen K, Schwarz MC, White JP, Luca VC, Fremont DH, et al. A Library of Infectious Hepatitis C Viruses with Engineered Mutations in the E2 Gene Reveals Growth-Adaptive Mutations That Modulate Interactions with Scavenger Receptor Class B Type I. J Virol. 2016; 90: 10499–10512. https://doi.org/10.1128/JVI.01011-16 PMID: 27630236

49. Catanese MT, Uryu K, Kopp M, Edwards TJ, Andrus L, Rice WJ, et al. Ultrastructural analysis of hepatitis C virus particles. Proc Natl Acad Sci U S A. 2013; 110: 9505–9510. https://doi.org/10.1073/pnas.1307527110 PMID: 23690609

50. Sabo MC, Luca VC, Prentoe J, Hopcraft SE, Blight KJ, Yi M, et al. Neutralizing Monoclonal Antibodies against Hepatitis C Virus E2 Protein Bind Discontinuous Epitopes and Inhibit Infection at a Postattachment Step. J Virol. 2011; 85: 7005–7019. https://doi.org/10.1128/JVI.00586-11 PMID: 21543495

51. Bankwitz D, Steinmann E, Bitzegeio J, Ciesek S, Friesland M, Herrmann E, et al. Hepatitis C virus hypervariable region 1 modulates receptor interactions, conceals the CD81 binding site, and protects conserved neutralizing epitopes. J Virol. 2010; 84: 5751–5763. https://doi.org/10.1128/JVI.02200-09 PMID: 20357091

52. Prentoe J, Gottwein JM, Scheel TKH, Jensen TB, Serre S, Bukh J. 82 DELETION OF HYPERVARIABLE REGION 1 (HVR1) OF E2 FROM HCV GENOTYPES 1–6 HAS DIFFERENTIAL EFFECT ON INFECTIVITY IN VITRO AND CAUSES INCREASED SUSCEPTIBILITY TO NEUTRALIZATION. J Hepatol. 2009; 50: S34.

53. Prentoe J, Verhoye L, Moctezuma RV, Buysschaert C, Farhoudi A, Wang R, et al. HVR1-mediated antibody evasion of highly infectious in vivo adapted HCV in humanised mice. Gut. 2015; 65: 1988–1997. https://doi.org/10.1136/gutjnl-2015-310300 PMID: 26589670

54. Munro JB, Gorman J, Ma X, Zhou Z, Arthos J, Burton DR, et al. Conformational dynamics of single HIV-1 envelope trimers on the surface of native virions. Science. 2014; 346: 759–763. https://doi.org/10.1126/science.1254426 PMID: 25298114

55. Sattentau QJ, Moore JP. Conformational changes induced in the human immunodeficiency virus envelope glycoprotein by soluble CD4 binding. J Exp Med. 1991; 174: 407–415. PMID: 1713252

56. Zimmerman B, Kelly B, McMillan BJ, Seegar TCM, Dror RO, Kruse AC, et al. Crystal Structure of a Full-Length Human Tetraspanin Reveals a Cholesterol-Binding Pocket. Cell. 2016; 167: 1041–1051.e11. https://doi.org/10.1016/j.cell.2016.09.056 PMID: 27881302

57. Neculai D, Schwake M, Ravichandran M, Zunke F, Collins RF, Peters J, et al. Structure of LIMP-2 provides functional insights with implications for SR-BI and CD36. Nature. 2013; 504: 172–176. https://doi.org/10.1038/nature12684 PMID: 24162852

58. Schneider CA, Rasband WS, Eliceiri KW. NIH Image to ImageJ: 25 years of image analysis. Nat Methods. 2012; 9: 671–675. PMID: 22930834

59. Schindelin J, Arganda-Carreras I, Frise E, Kaynig V, Longair M, Pietzsch T, et al. Fiji: an open-source platform for biological-image analysis. Nat Methods. 2012; 9: 676–682. https://doi.org/10.1038/nmeth.2019 PMID: 22743772

60. Catanese MT, Ansuini H, Graziani R, Huby T, Moreau M, Ball JK, et al. Role of Scavenger Receptor Class B Type I in Hepatitis C Virus Entry: Kinetics and Molecular Determinants. J Virol. 2009; 84: 34–43.

61. Schmidt TGM, Batz L, Bonet L, Carl U, Holzapfel G, Kiem K, et al. Development of the Twin-Strep-tag and its application for purification of recombinant proteins from cell culture supernatants. Protein Expr Purif. 2013; 92: 54–61. https://doi.org/10.1016/j.pep.2013.08.021 PMID: 24012791

62. Grove J, Nielsen S, Zhong J, Bassendine MF, Drummer HE, Balfe P, et al. Identification of a residue in hepatitis C virus E2 glycoprotein that determines scavenger receptor BI and CD81 receptor dependency and sensitivity to neutralizing antibodies. J Virol. 2008; 82: 12020–12029. https://doi.org/10.1128/JVI.01569-08 PMID: 18829747

63. Flyak AI, Ruiz S, Colbert MD, Luong T, Crowe JE Jr, Bailey JR, et al. HCV Broadly Neutralizing Antibodies Use a CDRH3 Disulfide Motif to Recognize an E2 Glycoprotein Site that Can Be Targeted for Vaccine Design. Cell Host Microbe. 2018; 24: 703–716.e3. https://doi.org/10.1016/j.chom.2018.10.009 PMID: 30439340

64. Neculai D, Schwake M, Ravichandran M, Zunke F, Collins RF, Peters J, Neculai M, Plumb J, Loppnau P, Pizarro JC, Seitova A, Trimble WS, Saftig P, Grinstein S, Dhe-Paganon S. Structure of LIMP-2 provides functional insights with implications for SR-BI and CD36. *Nature* (2013) 504 p. 172–6.

65. Lo Surdo P., Bottomley M.J., Calzetta A., Settembre E.C., Cirillo A., Pandit S., Ni Y.G., Hubbard B., Sitlani A., Carfi A. Mechanistic implications for LDL receptor degradation from the PCSK9/LDLR structure at neutral pH. Embo Rep. (2011) 12: 1300–1305.